UNIVERSITY OF OKLAHOMA

GRADUATE COLLEGE

ASSESSING PRECIPITATION DELINEATION CAPABILITIES OF SPACEBORNE RADARS

A THESIS

SUBMITTED TO THE GRADUATE FACULTY

in partial fulfillment of the requirements for the

Degree of

MASTER OF SCIENCE IN METEOROLOGY

By

MARESA SEARLS
Norman, Oklahoma
2022

ASSESSING PRECIPITATION DELINEATION CAPABILITIES OF SPACEBORNE RADARS

A THESIS APPROVED FOR THE
SCHOOL OF METEOROLOGY

BY THE COMMITTEE CONSISTING OF

Dr. Pierre Kirstetter, Chair

Dr. Jeffrey Basara

Dr. Greg Mcfarquhar

Acknowledgements

First and foremost, I would like to thank my advisor, Dr. Pierre Kirstetter, for his guidance, advice, and support throughout. I would also like to thank my committee members, Dr. Jeff Basara and Dr. Greg McFarquhar, for feedback on my thesis.

Additionally, thank you to NASA's Precipitation Measurement Mission Science Team for funding this research.

Finally, thank you to my family and friends for all of the support. Doing this research in the middle of a pandemic was difficult, but your support made it much easier and helped get me through it.

Table of Contents

List of Tables

List of Figures

Abstract

Spaceborne radars uniquely measure, provide the finest depiction of, and give the most accurate estimate of precipitation globally from space. The Global Precipitation Measurement (GPM) mission dual-frequency precipitation radar (DPR) is the successor to the Tropical Rainfall Measuring Mission (TRMM) precipitation radar (PR), expanding on its capabilities with a dual-frequency radar and coverage into the midlatitudes. The consistent ability to detect various precipitation magnitudes across satellite missions is critical to the study of global precipitation over various time periods. The precipitation delineation capabilities of spaceborne radars are characterized as functions of their reflectivity and the corresponding precipitation magnitude from the reference Ground Validation Multi-Radar/Multi-Sensor (GV-MRMS) over CONUS. The Heidke Skill Score, a measure of skill with respect to random chance, is computed to synthesize the capabilities of the spaceborne radars. This enables a finer depiction and interpretation of spaceborne radar capabilities than the bulk metrics widely used in the literature. Skill is more sensitive to changes in rain rate at lower rain rates and changes in reflectivity at higher rain rates. The TRMM-PR and GPM-DPR best delineate moderate precipitation while the GPM-KuPR detects precipitation with low to moderate skill. While both the TRMM-PR and GPM-DPR perform better than GPM-KuPR, the TRMM-PR performs better at lower reflectivity thresholds while the GPM-DPR performs better at higher reflectivity thresholds. Certain factors do not have a significant impact on the overall skill. Others have a significant impact, but the number of cases were small and did not greatly impact the overall skill. While the GPM-DPR struggles with the detection of precipitation, and the TRMM-PR performs the best overall, both the GPM-DPR and TRMM-PR have good delineation capabilities.

1 Introduction and Background

Water plays a crucial role on Earth, from transporting heat through the atmosphere and oceans, to causing devastation through extreme weather. Most importantly, water is vital for sustaining life. Precipitation is a primary source of fresh water and connects Earth's water and energy cycles. Therefore, knowing when, where, and how much precipitation is falling is of great importance to humanity (Skofronick-Jackson et al. 2017). Additionally, climate change is affecting the distribution of the world's water. In some areas, warmer temperatures will lead to more moisture and more intense precipitation, increasing flooding potential. In other areas, warmer temperatures will lead to increased drying and drought. Satellites, due to their quasi-global coverage, are used for global quantitative precipitation estimation (QPE) to study the water cycle.

Among spaceborne sensors, data from spaceborne radars help estimate the rate of water transfer within the Earth's atmosphere and on its surface, leading to improvement in Earth system modeling and analysis. Increased accuracy in global precipitation estimates improve climate model accuracy and effectiveness (NASA 2021).

Spaceborne radars, such as the instruments that were onboard the Tropical Rainfall Measuring Mission (TRMM) and are currently onboard the Global Precipitation Measurement (GPM) mission, use active sensing to provide unique profiling capabilities of precipitation (Hou et al. 2014; Stephens et al. 2002). Radars are acknowledged to provide the most accurate estimates of precipitation among space-based sensors, but their error structure is complex and a large component of their usefulness (Liao and Meneghini 2022; Porcacchia et al. 2019). Therefore, accurately detecting precipitation and delineating precipitation magnitudes is a necessary capability that is seldom evaluated but has implications for spaceborne constellations, global precipitation estimation, and the monitoring of the water cycle, among other applications. This

research introduces such an assessment, focusing on the capabilities of spaceborne radars to delineate precipitation magnitudes. Accurately doing so is key for research and applications and has a direct impact on products that are calibrated with spaceborne radars.

Working at the primary spaceborne radar QPE scale is necessary for such a quantitative and detailed characterization. The Ground Validation Multi-Radar/Multi-Sensor (GV-MRMS) is used for an independent and consistent reference precipitation for comparison and evaluation over the CONUS (Kirstetter et al. 2012, 2020) with the TRMM Precipitation Radar (PR) and the GPM Dual-frequency Precipitation Radar (DPR). Collective precipitation observations with ground-based and spaceborne sensors provide an opportunity for comparison of QPE, as the measurements are physically consistent through the identification of hydrometeors and estimation of particle size distribution.

The remainder of this section provides a background on the instruments used in this research, potential errors spaceborne radars must correct for, and the goals of this research. Section 2 describes the data and methods used. Section 3 has the results, section 4 discusses the results, and section 5 provides a summary and conclusions.

1.1 TRMM-PR

The TRMM was a joint satellite mission between the United States and Japan to provide the first detailed and comprehensive dataset of the distribution of rainfall over the tropics and subtropics (Kummerow et al. 1998). The mission was launched on 27 November 1997 and officially ended on 15 April 2015. It had an inclination angle of 35°. It originally was launched to an altitude of 350 km but was boosted to 403 km in 2001 to increase its lifespan. It was in a non-sun-synchronous orbit, meaning that the satellite would pass over a particular point at different times of day. This

allowed for the study of diurnal patterns of multiple variables. There were five instruments onboard, including the TRMM-PR.

The TRMM-PR was the first spaceborne instrument designed to provide three-dimensional maps of storm structure, giving information on the intensity and distribution of rain, rain type, storm depth, and height of the melting layer (NASA 2020a). It was a Ku band radar that operated at a frequency of 13.8 GHz, with a swath width of 247 km, a horizontal resolution of 5 km, and a 250 m range resolution. Its minimum detectable signal was 18 dBZ, corresponding to a rain rate of 0.7 mm hr^{-1}. The TRMM uses the Z-R relationship:

$$Z = aR^b \tag{1}$$

with a = 372.4 and b = 1.54.

1.2 GPM-DPR

The successor to the TRMM is the GPM mission. The GPM mission is an international satellite mission designed to set a new standard for precipitation measurement from space and provide a new generation of global precipitation observations in all parts of the world ever 3 hours (Hou et al. 2014). The GPM mission consists of approximately 12 constellation satellites. The satellite used for calibration and the satellite which has the GPM-DPR onboard is the GPM Core Observatory (CO). The GPM CO was launched on 27 February 2014, at an altitude of 407 km. It covers areas between 68° N and S. It is in a non-sun-synchronous orbit and has two instruments onboard, including the GPM-DPR.

The GPM-DPR is an updated version of the TRMM-PR. The GPM-DPR has both Ku-band and Ka-band precipitation radars (GPM-KuPR and GPM-KaPR, respectively), coaligned such that

the footprint location on the Earth is the same (NASA 2020b). The GPM-KuPR operates at a frequency of 13.6 GHZ with a swath width of 245 km. The GPM-KaPR operates at a frequency of 35.5 GHz with a swath width of 120 km. Both radars have a 5 km horizontal resolution and a 250 m range resolution, although the GPM-KaPR has a 500 m range resolution in its high sensitivity mode. The GPM-DPR has a minimum detectable signal of 12 dBZ for the GPM-KaPR and 18 dBZ for the GPM-KuPR, corresponding to rain rates of 0.2 mm hr^{-1} and 0.5 mm hr^{-1}, respectively. For the GPM-DPR, rain rate is found using (1), but with a = 200 and b = 1.6. Table 1 provides a comparison between the TRMM-PR and GPM-DPR.

Table 1: Comparison of characteristics for the GPM-KaPR, GPM-KuPR, and TRMM-PR.

Instrument	GPM-KaPR	GPM-KuPR	TRMM-PR (Post Boost)
Inclination Angle	68°	68°	35°
Altitude (km)	407	407	403
Frequency (GHz)	35.5	13.6	13.8
Swath Width (km)	120	245	247
Horizontal Resolution (km)	5	5	5
Range Resolution (m)	250 (500 in high sensitivity mode)	250	250
Minimum Detectable Signal	12 dBZ (0.2 mm hr^{-1})	18 dBZ (0.5 mm hr^{-1})	18 dBZ (0.7 mm hr^{-1})

1.3 GV-MRMS

The MRMS system was built at the National Severe Storms Laboratory using parts from the Warning Decision System-Integrated Information (see Lakshmanan et al. 2007) and the National Mosaic and Multi-Sensor QPE (Zhang et al. 2011) systems. The GV-MRMS is derived from the MRMS and is designed for comparison with satellite precipitation products. The GV-MRMS domain is from 20° to 55° N and from 60° to 130° W. It has a horizontal resolution of 0.01° both latitudinally and longitudinally. This corresponds to about 1.11 km in the north-south direction. In

the east west direction, the resolution is about 1 km at the southern bound and 0.6 km at the northern bound. The temporal resolution is 2 minutes. The GV-MRMS consists of 146 S-band dual-polarization Weather Surveillance Radar-1998 Doppler (WSR-88D) radars and 30 Canadian C-band radars, as well as over 7000 hourly rain gauges (Zhang et al. 2016). Figure 1 illustrates the locations of the radars and rain gauges.

Gauge-based corrections, quality and quantity controls, and resampling procedures are applied to standardize the product and filter out less trustworthy GV-MRMS estimates, described in detail in Kirstetter et al. (2012, 2014, 2015a, 2020). In particular, a radar quality index (RQI) product is used to minimize potential error. RQI values of 1 have very little bias and is the threshold used for the data in this study (for more information on RQI, see Zhang et al. 2012).

1.4 Considerations for Spaceborne Radars

Spaceborne radars use the same active remote sensing principles as ground-based radars, but scan in the vertical and travel across regions at a velocity of several km s^{-1}. In a horizontal scan, such as those performed by ground-based radars, a beam will typically only contain one type of precipitation process. A vertical beam, however, contains multiple precipitation processes.

Additionally, to have a reasonable horizontal resolution, higher frequency bands (Ku and Ka) than those in the ground-based system (S and C bands) are used. These higher frequency bands are more prone to attenuation, which impacts precipitation delineation capabilities, and must be corrected (Iguchi 2003). The measured reflectivity (Z_{mo}) of a radar is related to attenuation (A) at range r by:

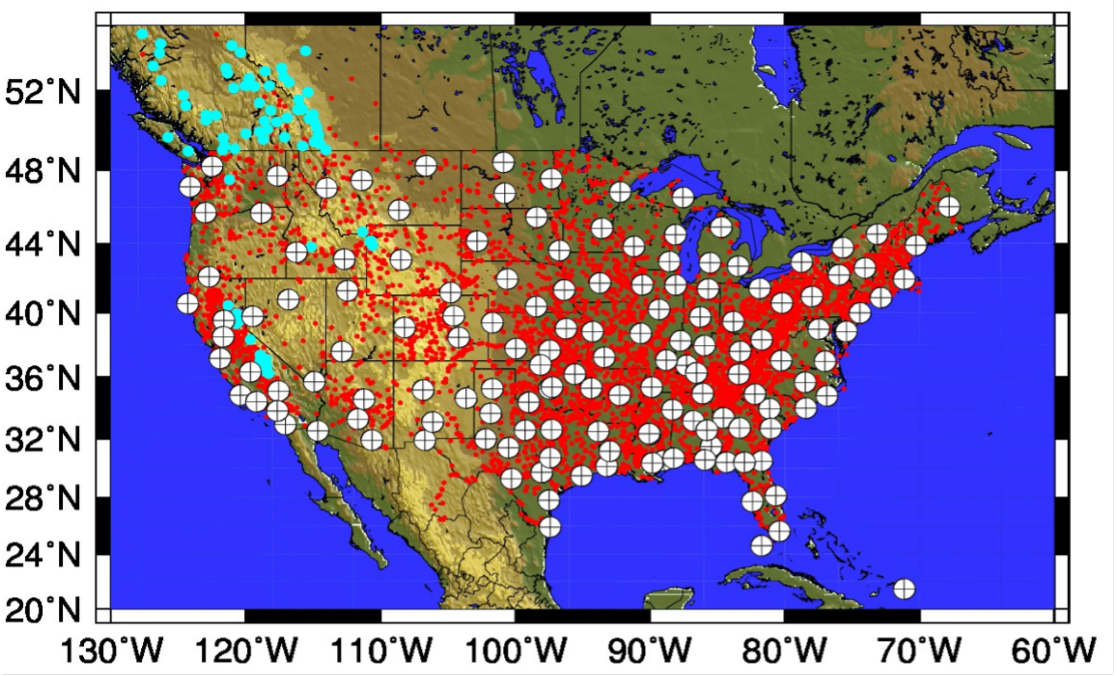

Figure 1: Locations of WSR-88D Radars (white dots), Canadian C-band radars (blue dots), and rain gauges (red dots). From Kirstetter et al. 2015b.

$$Z_{m0}(r) = Z_e(r)A(r) \tag{2}$$

where Z_e is the effective reflectivity. The effective reflectivity is defined as:

$$Z_e = \frac{\lambda^4}{\pi^5 |K|^2} \int \sigma_b(D) N(D) dD \tag{3}$$

where D is diameter of the precipitation particle, λ is the wavelength of the radar, K is a constant based on the refractive index, σ_b is the backscattering cross section and N(D) is the particle size distribution (PSD). The PSD can be parameterized as:

$$N(D) = N^* n(D; D^*) \tag{4}$$

where n is a function of D and N^* and D^* are unknown parameters. In a single frequency radar, such as the TRMM-PR, N(D) is characterized by a single parameter, say D^*, and Z_e and D^* are in a one-to-one correspondence. Since these are in a one-to-one correspondence, knowing D^* obtains Z_e, allowing for (2) to be solved for attenuation. However, in nature, PSD cannot be sufficiently characterized by a single parameter, leading to errors and biases. In a dual-frequency radar, such as the GPM-DPR, N(D) can be characterized by 2 parameters, leading to more accurate attenuation correction (Iguchi et al. 2021).

Both the TRMM-PR and GPM-DPR are also subject to errors in rainfall retrievals that are associated with the reflectivity-to-precipitation intensity conversion, relating to incorrect physical assumptions on precipitation classification of convective versus stratiform and particle size distribution (Kirstetter et al. 2020). In the single-frequency radars, precipitation is classified as either convective or stratiform using two methods, the vertical profile method (V-method) and horizontal pattern method (H-method). In the V-method, the vertical profile of the radar reflectivity factor is examined to see if it satisfies certain conditions which are typical to its profile when a bright band exists. If a bright band is detected, the rain type is classified as stratiform if the reflectivity factor does not exceed a special convective threshold of 46 dBZ. When a bright band is not detected and the reflectivity factor exceeds a convective threshold of 40 dBZ, the rain type is classified as convective. In the H-method, the horizontal texture of the maximum value of the reflectivity factor corrected for attenuation by the non-precipitation particles in the rain region is examined. A modified University of Washington convective/stratiform separation method (see Steiner et al. 1995; Yuter and Houze 1997) is used to the horizontal extent of this maximum value pixel. When this pixel either exceeds a convective threshold of 40 dBZ or it stands out against the surrounding area, the rain type for this pixel and the pixels adjacent to it are classified as

convective. The DFR_m method is used with the dual-frequency radar. In this method, the difference between the reflectivity in the Ku-band and Ka-band is used to determine if a bright band is present. Like the V-method, if a bright band is detected, the precipitation type is stratiform unless the reflectivity exceeds the special convective threshold (46 dBZ) and, if no bright band is detected, the precipitation type is convective if the reflectivity exceeds 40 dBZ (Iguchi et al. 2021).

In addition to errors associated with attenuation and precipitation type, other error sources include contamination by surface backscatter and sub-footprint precipitation variability (Wolff and Fisher 2008; Iguchi et al. 2009; Kirstetter et al. 2015a).

1.5 Goals

Numerous studies have evaluated space-based estimates of precipitation over different areas, climatologies, sampling conditions, and intensities to improve their usability (e.g., Kirstetter et al. 2015a; Lasser et al. 2019; Liu et al. 2022; Valdivia et al. 2022). However, the wide use of bulk metrics, such as correlation coefficient or mean squared error, to assess performance provides limited insight due to the computation of these metrics over a variety of sampling and precipitation characteristics, leading to uncertainties and a depiction of average properties (Clark et al. 2021; Kirstetter et al. 2020). Progress in precipitation estimation and application requires more than an overall assessment to deal with varying performances of precipitation products. This calls for a more informative assessment by conditioning it according to relevant elements driving the estimate performance. This research assesses the precipitation magnitude delineation capabilities at a finer scale (i.e., at a certain precipitation rate and reflectivity) than that provided by bulk metrics.

Additionally, this research compares the two generations of spaceborne radars to determine the potential usability of the products to create a continuous global precipitation climatology. It also assesses various factors, such as precipitation classification (stratiform or convective), region,

zenith angle, land type, the presence of the bright band, and shallow rain, and how they affect the precipitation delineation capabilities of the spaceborne radars.

2 Data and Methods

2.1 GV-MRMS Matched Pairs

Matched pairs of the GV-MRMS and spaceborne radars are created. Figure 2 illustrates how the GV-MRMS creates these matched pairs. Raw data is processed using science algorithms to produce calibrated, swath-level instrument data. Other algorithms are used to compute geophysical parameters at the swath-level resolution. The GV-MRMS products closest in time to the satellite local overpass are used, then a block GV-MRMS pixel is computed to match each spaceborne radar pixel to compute reference rainfall rate. The spaceborne radar footprints are then overlaid on the reference to create the matched pairs (Kirstetter et al. 2012, 2020). This research utilizes approximately 1.5 million matched pairs from May to October of 2011 from the TRMM-PR and 2 million matched pairs from May of 2014 to October of 2016 from the GPM-DPR (Tropical Rainfall Measuring Mission 2011; Iguchi and Meneghini 2017).

2.2 Heidke Skill Score

Bulk metrics (e.g., mean squared error, correlation coefficient) are often used to quantify the accuracy of spaceborne radars. However, these often can contain significant uncertainties due to outliers skewing the metrics. The Heidke Skill Score (HSS) can be used to provide a finer depiction of delineation capabilities. The HSS quantifies precipitation delineation capabilities relative to that of random chance. The score ranges from $-\infty$ to 1. Positive scores represent at least some delineation skill, while negative scores indicate negative skill with respect to random chance. A score of 0 represents no skill while a score of 1 indicates perfect delineation skill with respect to random chance.

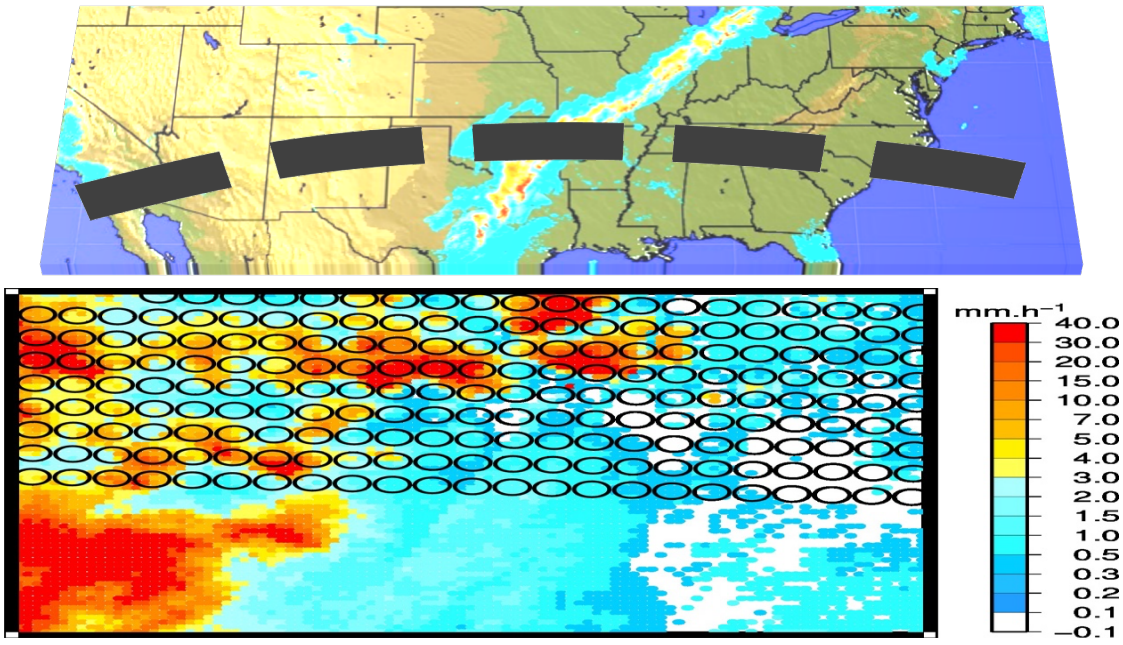

Figure 3: Overpass of satellite with zoomed area showing variability and spatial distribution of precipitation within the footprints (circles). Adapted from Kirstetter et al. 2015a.

To calculate HSS, the number of hits (H), misses (M), false alarms (F), and correct rejections (C) must be found. A hit is defined as when both the spaceborne radar and reference GV-MRMS meet a precipitation magnitude threshold, miss as when the GV-MRMS meets the threshold while the spaceborne radar does not, false alarm as when the spaceborne radar meets it but the GV-MRMS does not, and correct rejection as when neither meets the threshold. Table 2 provides a contingency table for determining these. The HSS is then calculated as (Brier and Allen 1951):

$$HSS = \frac{2(HC - FM)}{F^2 + M^2 + 2HC + (F + M)(H + C]} \quad (5)$$

Note, the score is calculated for areas with a sample size greater than 30, and that the GPM-KaPR is not used due to an insufficient sample size.

Table 2: Contingency Table for determining hits, misses, false alarms, and correct rejections for the Heidke Skill Score.

Reference rain rate threshold met? / **Spaceborne radar reflectivity threshold met?**	**Yes**	**No**
Yes	H	F
No	M	C

As traditionally employed, HSS is a scalar measure of skill (Conner and Petty 1998). The HSS has been used to characterize the performance of spaceborne radars in detecting rain from no rain with respect to a reference data set using a predefined threshold (e.g., Kirstetter et al. 2014). However, the HSS changes based on what was used as the predefined threshold. Thus, it is extended in this research by examining the exceedance relative to a range of rainfall thresholds. The HSS is computed and plotted as a continuous bivariate function of the continuously varying rainfall rate thresholds based on GV-MRMS and reflectivity thresholds estimated by spaceborne radars. It allows for the interpretation of precipitation magnitude delineation capabilities for various combinations of precipitation situations and spaceborne radar observations. The maximum skill found across all GV-MRMS thresholds is independent of any bias in the spaceborne radar retrievals (Chiu and Petty 2006).

Higher values of HSS indicate improved delineation of rain rate and reflectivity magnitudes. Good delineation capabilities are defined as scores greater than 0.40. Scores between 0.20 and 0.40 indicate moderate delineation skills, while positive scores less than 0.20 indicate at least some

delineation skill. The spaceborne radar reflectivity (reference rain rate) that maximizes the HSS as a function of any given rain rate (reflectivity) can be plotted as a line in a 2D-HSS plot.

3 Results

3.1 General Performance

Figure 3 shows the 2D-HSS bivariate histogram plots for each radar. Note, that this data includes all precipitation classifications (stratiform and convective), encompasses all zenith angles, and uses data from all latitudes available (tropical and midlatitudes), and all land types. It is also not restricted to only when the bright band or shallow rain is or is not detected. TRMM-PR data does not include the coastal surface type, and is restricted to less than 37° N, so 2D-HSS bivariate histograms for the GPM-DPR and GPM-KuPR for latitudes less than 37° N without the coastal surface type are included. Reference rain rates are on the x-axis, and spaceborne radar reflectivity is on the y-axis. HSS values are indicated by the contour colors. Contour lines provide quantitative values of HSS. The solid (dashed) grey line represents the maximum HSS for varying spaceborne radar reflectivity values (reference rain rates) for a given reference rain rate (reflectivity). When these lines are more vertically oriented, the delineation is more sensitive to changes in reference rain rate. It is more sensitive to changes in spaceborne radar reflectivity when the lines are more horizontally oriented. Contours closer together indicates that the skill is more sensitive to changes than when the contours are spaced further apart.

3.1.1 TRMM-PR

Figure 3a contains the HSS histogram for the TRMM-PR. The distribution of scores indicates that the TRMM-PR has good delineation capabilities over a wide range of rainfall rate and reflectivity conditions. Scores vary across the rain rate and reflectivity space. Conditions associated with lower scores are reflectivity above 40 dBZ and rain rates less than 2 mm hr^{-1}. Below approximately 30

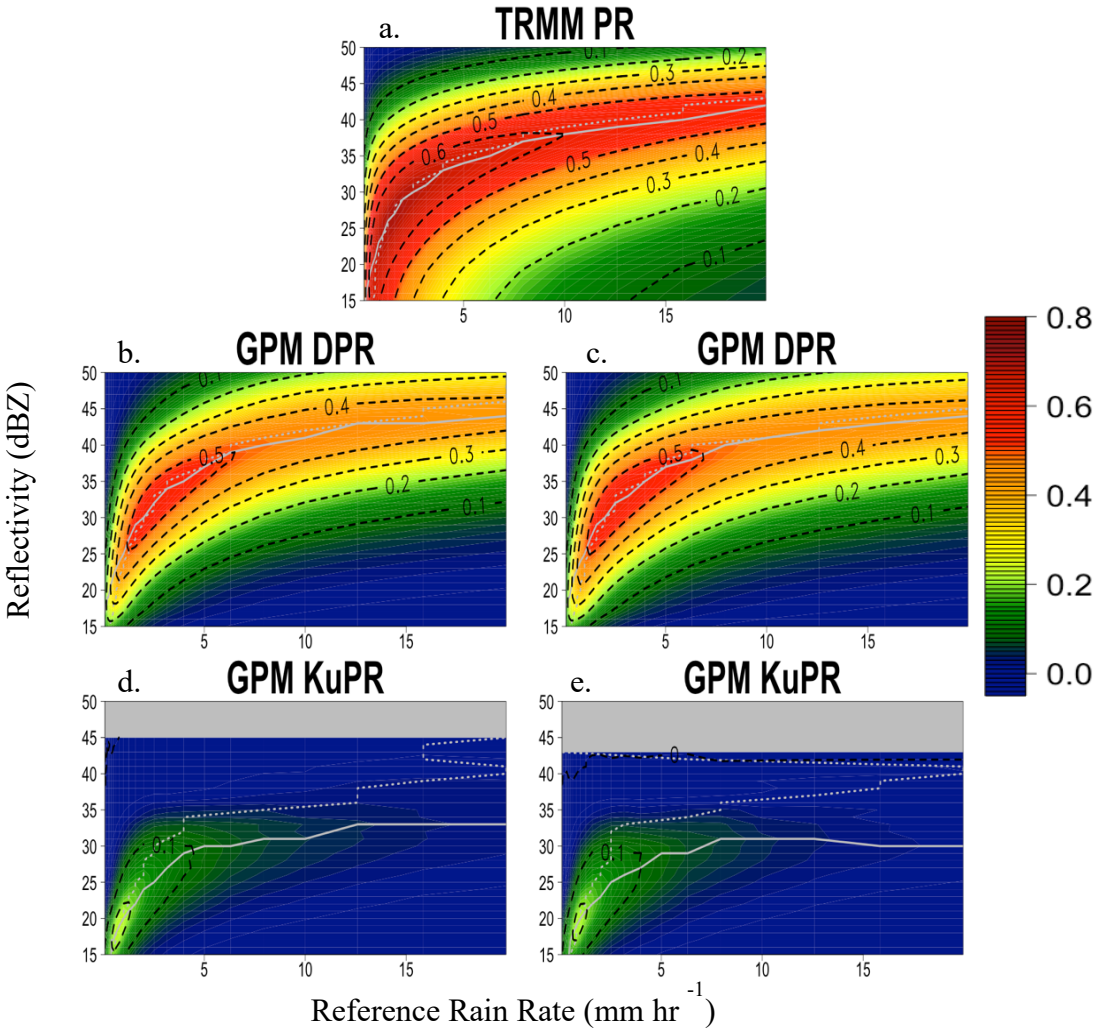

Figure 5: 2D-HSS bivariate histograms for the TRMM-PR (a), GPM-DPR (b), and GPM-KuPR (d). (c) and (e) are the same as (b) and (d), respectively, but excluding coastal surfaces and latitudes greater than 37° N.

dBZ, scores increase with increasing rain rate, reaching a maximum between about 2.5 and 5 mm hr^{-1}, then decrease with increasing rain rates. Above 30 dBZ, scores continue to gradually increase with increasing rain rate, although the range of reflectivity thresholds associated with moderate and good delineation capabilities slightly decreases at higher reference rain rates.

The TRMM-PR HSS reaches its maximum of about 0.7 at a reference rain rate threshold of 1.58 mm hr^{-1} and reflectivity threshold of 26 dBZ. Scores associated with precipitation detection

(i.e., reflectivity around 18 dBZ and very low rain rates) are around 0.6. As expected, the reflectivity value associated with a given delineation skill increases with rainfall magnitude before reaching a plateau (e.g., the maximum HSS curves (grey lines)).

3.1.2 GPM-DPR

Figure 3b contains the HSS histogram for the GPM-DPR. Like the TRMM-PR, the distribution of scores shows that the GPM-DPR also has delineation capabilities over a wide range of rainfall rate and reflectivity conditions, although at a lesser skill. Also similar to the TRMM-PR, the GPM-DPR has an area of lower scores that corresponds very low rain rates less than 1 mm hr^{-1} and reflectivity greater than about 40 dBZ. Another similarity to the TRMM-PR is that scores increase then decrease with increasing rain rate for a given lower reflectivity value, while the scores gradually increase with increasing rain rate for higher reflectivity values. The GPM-DPR reaches its maximum score of 0.56 for a reference rain rate of 2.51 mm hr^{-1} and a reflectivity of 31 dBZ.

Figure 3c depicts the GPM-DPR skill when restricted to latitudes less than 37° N and no coastal surfaces. The distribution of scores is very similar to when these restrictions are not included. The area of scores greater than 0.5 is slightly larger, but the range of reflectivity thresholds associated with positive scores is slightly smaller. The maximum skill is marginally greater, 0.57, at the same rain rate and reflectivity of 2.51 mm hr^{-1} and 31 dBZ, respectively.

3.1.3 GPM-KuPR

Figure 3d contains the 2D-HSS for the GPM-KuPR. Note that there is an insufficient sample size above reflectivity values of 45 dBZ across all rain rates. The GPM-KuPR has its best performance near the nominative sensitivity of the instrument (i.e., the minimum detectable reflectivity of 18 dBZ), although the scores in this area are rather low (around 0.20). The scores near 0 as the reference rain rate increases. This also occurs across all rain rates for reflectivity greater than

approximately 35 dBZ. The GPM-KuPR reaches its maximum score of 0.23 at a reference rain rate of 0.79 mm hr^{-1} and reflectivity of 18 dBZ.

Figure 3e is the histogram for no coastal surfaces with latitude less than 37° N. Similar to the GPM-DPR, the distribution of the scores is similar to that without these restrictions. The maximum score, however, is marginally lower than the previous maximum reached, at 0.22. This maximum is reached at a rain rate of about 1 mm hr^{-1} and reflectivity of 19 dBZ.

3.2 Precipitation Classification

Figure 4 illustrates the 2D-HSS histogram plots for the GPM-DPR and TRMM-PR when precipitation is classified as either stratiform or convective by the spaceborne radar. The left plots are for the GPM-DPR while the right plots are for the TRMM-PR. The top plots are when precipitation is classified as stratiform, and the bottom plots are when it is classified as convective. The Precipitation is classified as either convective or stratiform using the V-method and H-method for the TRMM-PR, while the DFR_m method is used for the GPM-DPR. Precipitation classification aims at distinguishing various precipitation types associated with different processes and rates. In particular, the relation between radar reflectivity and precipitation rates varies with types (e.g., Kirstetter et al., 2015a), so it is important to examine the magnitude delineation capabilities for each type. Note, the GPM-DPR will now be the focus of the GPM radars as it has a much higher overall score compared to the GPM-KuPR. Additionally, the sample size of the GPM-KuPR decreases significantly. Also note that data with coastal surfaces will be used with the GPM-DPR.

3.2.1 Stratiform

Figure 4a depicts the 2D-HSS for the GPM-DPR for cases with stratiform precipitation. As expected, the highest scores occur at lesser rain rates and moderate reflectivity values. Compared

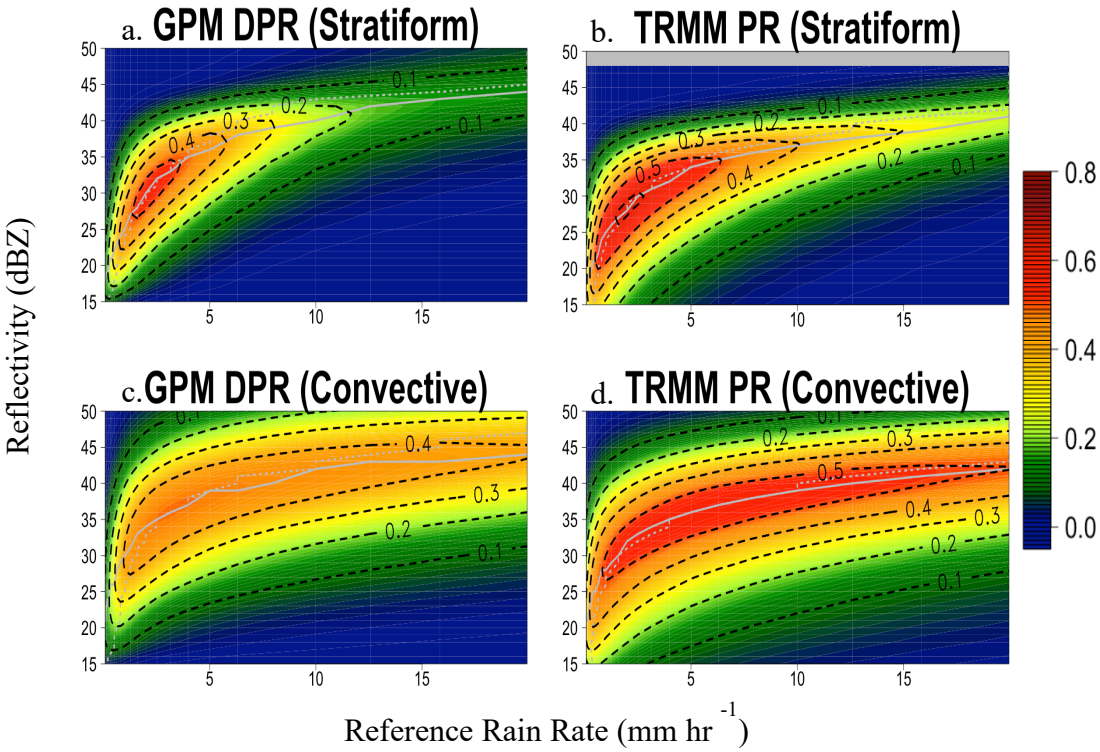

Figure 7: 2D-HSS bivariate histograms for the GPM-DPR (left) and TRMM-PR (right) for stratiform (top) and convective (bottom) cases.

to the general performance, the area of scores greater than 0.5 is smaller. Also as expected, HSS values decrease with increasing rain rates above about 5 mm hr^{-1}. At 35 dBZ, for example, scores are greater than 0.4 at 5 mm hr^{-1}, but near 0.1 at 20 mm hr^{-1}. The GPM-DPR reaches a maximum score of 0.53 for a precipitation rate of approximately 2 mm hr^{-1} and reflectivity of 29 dBZ.

Figure 4b shows the 2D-HSS for the TRMM-PR for stratiform precipitation. Similar to the GPM-DPR, the TRMM-PR has higher scores associated with lower rain rates and moderate reflectivity values. The TRMM-PR also has a smaller area of scores associated with the highest delineation capabilities compared to its general performance. The place where the maximum score occurs is very similar to the GPM-DPR, but the maximum score is greater. The TRMM-PR has its maximum capabilities at a rain rate of about 2 mm hr^{-1} and reflectivity of 27 dBZ, reaching a score of approximately 0.61.

3.2.2 Convective

Figure 4c has the 2D-HSS for convective precipitation cases with the GPM-DPR. Although the maximum score is only 0.48, occurring at about 3.15 mm hr^{-1} and 35 dBZ, the score does not rapidly decrease with increasing rain rate. At higher reflectivity values, such as around 45 dBZ, the score slightly increases with increasing rain rate. When compared to its general performance, however, the reflectivity range associated with good delineation capabilities (scores greater than 0.4) at higher rain rates is less than the general performance.

Figure 4d is the 2D-HSS for convective cases with the TRMM-PR. Expectedly, the scores remain high at higher rain rates. Again, however, the range of reflectivity associated with scores greater than 0.5 at higher rain rates is less than that of the general performance. The maximum score for the TRMM-PR occurs at a slightly higher rain rate but lower reflectivity than the GPM-DPR. The score reaches about 0.55 at a rain rate of about 4 mm hr^{-1} and a reflectivity of 34 dBZ.

3.3 Region

Figure 5 shows the performance of the GPM-DPR in both the tropics and the midlatitudes. Precipitation regimes and associated rates change with regions. Different regions have differing dominant precipitation types. For example, the tropics will have more convective precipitation than the midlatitudes. For this research, the tropics is defined as latitude less than 37°. As such, this section does not include the TRMM-PR, and instead focuses on the GPM-DPR.

3.3.1 Tropics

Figure 5a has the delineation skill when the data is from only over the tropics. The scores do not differ greatly from the overall skill. The maximum delineation skill is slightly higher in the tropics

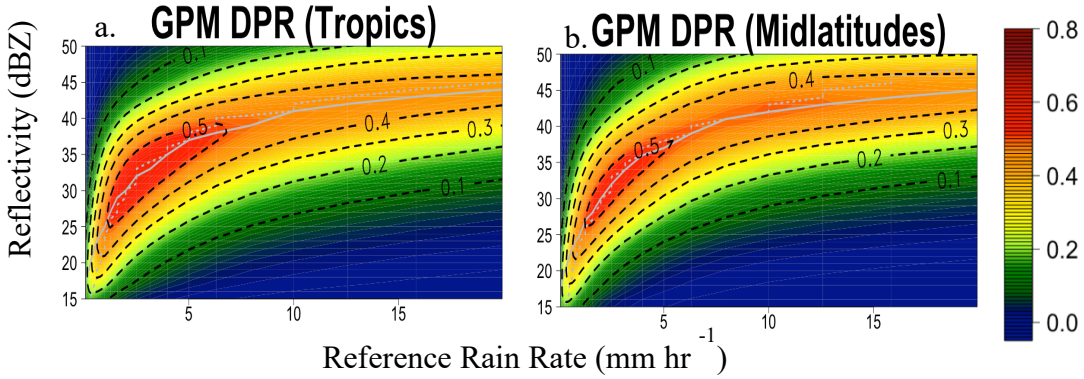

Figure 9: 2D-HSS bivariate histograms for the GPM-DPR in the tropics (a) and midlatitudes (b).

compared to overall, at 0.57, occurring at the same reference rain rate and reflectivity of 2.51 mm hr^{-1} and 31 dBZ, respectively.

3.3.2 Midlatitudes

Figure 5b has the skill for the midlatitudes. Much like the tropics, the scores do not greatly differ from the overall skill. The area of skill greater than 0.5 is slightly smaller than the area of this skill overall, and much smaller than in the tropics. Also like the tropics, the maximum score occurs at the same reference rain rate and reflectivity (2.51 mm hr^{-1} and 31 dBZ, respectively), but the maximums score is only about 0.54, less than both that of over the tropics and overall.

3.4 Zenith Angle

Figure 6 contains the 2D-HSS histogram plots for the GPM-DPR when the zenith angle, the angle at which the radar beam was at when a measurement was taken with respect to the nadir point (when the beam is vertical), is near the nadir (near nadir) and when the zenith angle is far from the nadir (far nadir). The dependance of precipitation retrievals with the zenith angle has been documented in the literature (e.g., Iguchi et al. 2000). Since the GPM-DPR and TRMM-PR have

different swath widths, the range of zenith angles is different, and the zenith angles corresponding to near nadir and far nadir will be different. The range of zenith angles for the GPM-DPR is from near 0° to about 9.1°, while the TRMM-PR goes to 18°. For this research, the near and far nadir will be defined as within 0.75° of the minimum and maximum zenith angles. For the GPM-DPR, this corresponds to angles less than 0.75° and angles greater than 8.35°, while it corresponds to angles less than 0.75° and angles greater than 17.25° for the TRMM-PR.

3.4.1 Near Nadir

Figure 6a is the 2D-HSS for the near nadir angles for the GPM-DPR. The skill at the near nadir angles is very similar to the overall skill, although the area of scores greater than 0.5 extends to slightly lower reflectivity values. The maximum skill is slightly higher than the skill with the general performance, at 0.57. This skill is reached at a higher reflectivity of 33 dBZ and rain rate of 3.16 mm hr^{-1}.

Figure 6b shows the 2D-HSS for the TRMM-PR. Like the GPM-DPR, the skill for near nadir angles is similar to the overall skill. Also like the GPM-DPR, the maximum skill is slightly greater than that of the general performance. It reaches a maximum score of about 0.71 at a reflectivity of 26 dBZ and a reference rain rate of 1.58 mm hr^{-1}.

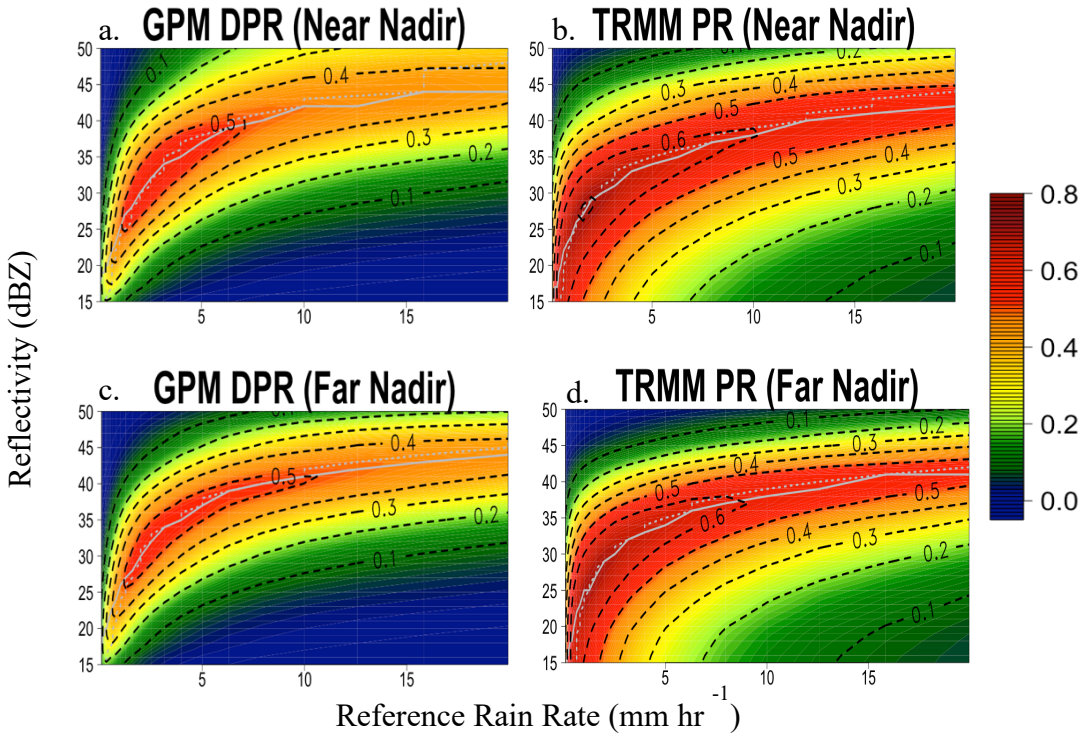

Figure 11: 2D-HSS bivariate histograms for the GPM-DPR (left) and TRMM-PR (right) for near nadir (top) and far nadir (bottom) angles.

3.4.2 Far Nadir

Figure 6c is the 2D-HSS histogram for the far nadir angles for GPM-DPR, while figure 6d is for the TRMM-PR. Again, with both radars, the skill at far nadir angles is similar to the general performance. The area of skill for the GPM-DPR, especially noticeable at scores greater than 0.5, is elongated, with the area of scores greater than 0.5 almost reaching rain rates of 10 mm hr^{-1}. The maximum score, however, is slightly less than that of the overall performance. The skill for far nadir angles reaches a maximum score of 0.55 at a rain rate of 2.51 mm hr^{-1} and reflectivity of 31 dBZ. The area of skill for the TRMM-PR, is thinner than that of both the general performance and near nadir angles. This can be seen especially well in the area of skill greater than 0.5. For example, at a rain rate of 20 mm hr^{-1}, this area goes from about 38 to 45 dBZ in both the general performance

and near nadir cases, but only goes from 38 to 40 dBZ in the case of far nadir. The far nadir angles also yield a lower score of .69 at 1.58 mm hr^{-1} and 26 dBZ.

3.5 Surface Type

Figure 7 contains the 2D-HSS histogram plots for the GPM-DPR and the TRMM-PR for different surface types. The surface cross-section is important to estimate accurately for the profiling algorithms and the correction of attenuation, which has direct impact on estimating precipitation rates and delineating magnitudes. The four different surface types are land, ocean, inland water, and coast. As stated previously, the TRMM-PR does not have a coast surface type, so the GPM-DPR will be the focus for the coastal surface type.

3.5.1 Land

Figure 7a is the 2D-HSS histogram for the land surface type for the GPM-DPR. The area of positive scores, in particular the area of scores greater than 0.5 is slightly greater than the area for the general performance of the radar. The area greater than 0.5 near 37 dBZ is expanded from a rain rate of about 6 mm hr^{-1} to about 7.5 mm hr^{-1}. At a rain rate around 2 mm hr^{-1}, it is expanded from 26 dBZ to 25 dBZ. The maximum score increases to about 0.57, occurring at the same rain rate and reflectivity as the maximum score for the general performance, 2.51 mm hr^{-1} and 31 dBZ, respectively. Figure 7b is for the TRMM-PR. Like the GPM-DPR, the area of scores greater than 0.5 expands, specifically in its range of reflectivity values it covers at the higher rain rates. At 20 mm hr^{-1}, the scores range from 38 dBZ to about 45 dBZ, compared to 39 dBZ to about 44 dBZ in the general performance. The area greater than 0.6, however, is very similar to the general performance. The maximum score also stays the same, 0.7, occurring at the same reflectivity and rain rate, 26 dBZ and 1.58 mm hr^{-1}, respectively.

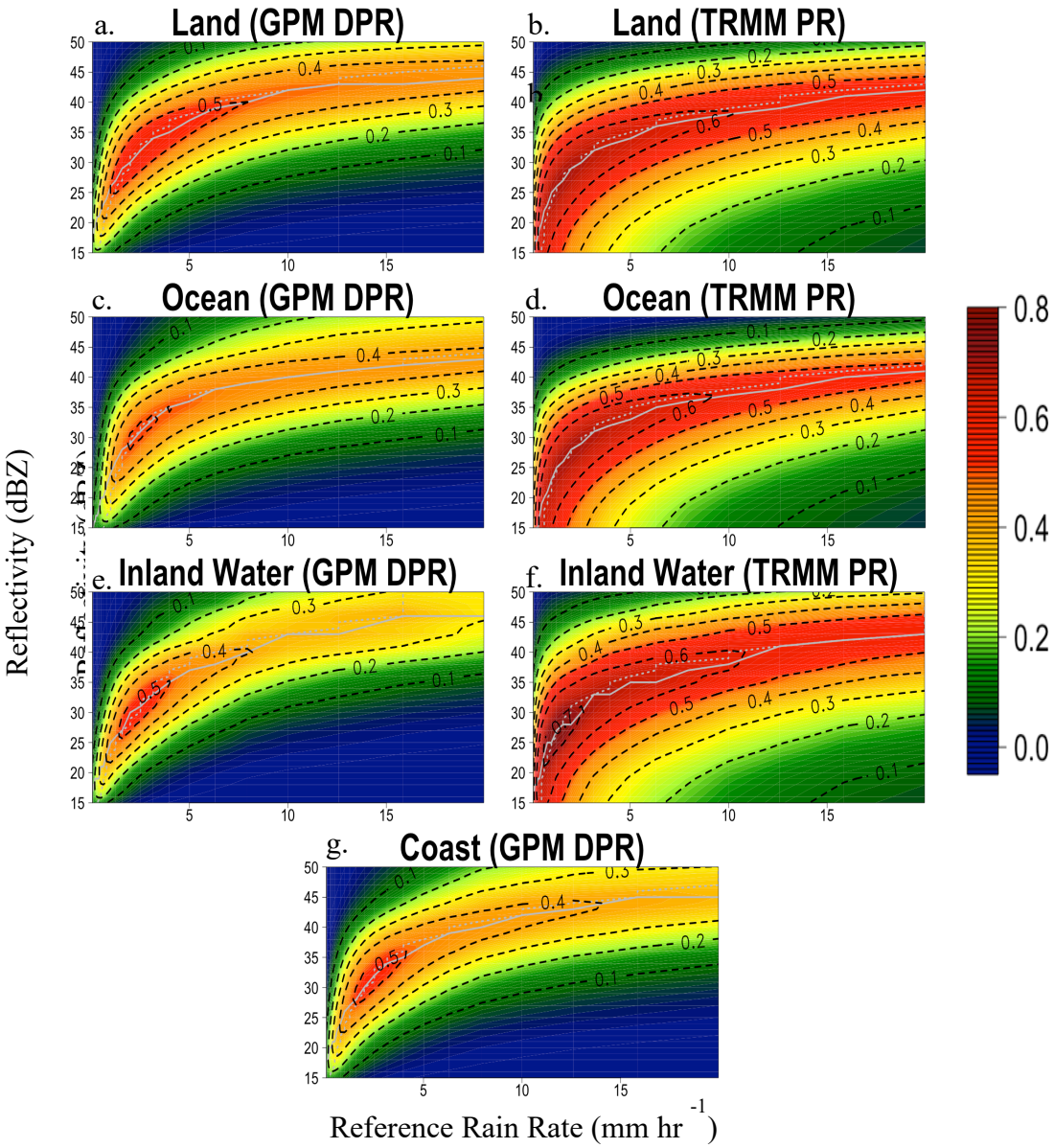

Figure 13: 2D-HSS bivariate histograms for land (a), ocean (c), inland water (e), and coast (g) surfaces for the GPM-DPR. (b), (d), and (f) are the same as (a), (c), and (e) but for the TRMM-PR.

3.5.2 Ocean

Figures 7c and d are the histograms for the ocean surface type. For the GPM-DPR, the area associated with positive scores slightly decreases overall, and even greater for the area of scores over 0.4. At higher rain rates, the range of reflectivity values associated with scores greater than

0.4 goes from about 41 to 47 dBZ in the general performance to about 41 and 45 dBZ for ocean surface cases. The area of scores greater than 0.5 greatly decreases. The maximum score also decreases to about 0.51, occurring at a slightly lesser reflectivity of 30 dBZ but the same rain rate of 2.51 mm hr^{-1}.

Focusing on the TRMM-PR, a similar pattern can be seen. At high rain rates, the area of scores greater than 0.5 decreases from a reflectivity range of about 39 to 44 dBZ in the general performance to about 40 to 42 dBZ for the ocean surface type. The area greater than 0.6 also decreases. In the general performance, this area almost reaches 10 mm hr^{-1} (at about 35 dBZ), but it only reaches about 8 mm hr^{-1} for the ocean. The maximum score, however, stays the same (but at a higher rain rate and reflectivity). It reaches about 0.7 at a rain rate of 1.99 mm hr^{-1} and reflectivity of 27 dBZ.

3.5.3 Inland Water

Figure 7e is the 2D-HSS for the GPM-DPR for inland water while 7f is for the TRMM-PR. Focusing on the GPM-DPR, the area of scores associated with at least some delineation skill (positive scores) greatly decreases. The area of scores greater than 0.4 does not extend past a rain rate of 8 mm hr^{-1}. Interestingly, the area of scores greater than 0.5 is larger for inland water than for ocean, but still not as large as the overall performance. The maximum score for inland water is greater than for ocean, but still less than the overall performance. The GPM-DPR for inland water reaches a maximum score of about 0.55 at a rain rate of 2.51 mm hr^{-1} and reflectivity of 30 dBZ.

For the TRMM-PR, the area of positive scores increases. At high rain rates, the area of scores greater than 0.5 expands from a reflectivity range of 39 to 44 dBZ to 39 to 46 dBZ. The area greater than 0.6 extends past a rain rate of 10 mm hr^{-1}. At rain rates around 2 mm hr^{-1} and reflectivity values around 27 dBZ, there is an area of scores greater than 0.7, greater than the maximum score

reached in the general performance. The TRMM-PR for inland water reaches a maximum score of 0.74 at a reflectivity of 26 dBZ and rain rate of 1.26 mm hr^{-1}.

3.5.4 Coast

Figure 7g is the 2D-HSS for the GPM-DPR for coastal surfaces. Like inland water, the area of positive scores is smaller than the general performance. The area of scores greater than 0.4 also does not fully extend across the higher rain rates, but it does reach a higher rain rate than inland water, reaching about 13 mm hr^{-1}. Also like inland water, the area of scores higher than 0.5 is larger than that for the ocean but less than the general performance. It reaches a maximum score of 0.53 at a rain rate of 2.51 mm hr^{-1} and reflectivity of 31 dBZ.

3.6 Bright Band

Figure 8 depicts the 2D-HSS for the GPM-DPR and TRMM-PR for when the bright band is and is not detected by the spaceborne radar. The bright band is the area of higher reflectivity associated with the melting layer and must be corrected.

3.6.1 Bright Band Only

Figure 8a shows the 2D-HSS histogram when bright band is detected for the GPM-DPR. The area of scores associated with some delineation skill is much smaller when the bright band is detected/present. The scores also decrease with increasing rain rate, instead of staying fairly constant as the rain rate increases at higher reflectivity values. The area of scores greater than 0.5 is also much smaller than the general performance, and the skill near the nominative sensitivity of the instrument is less than the general performance. The maximum skill decreases slightly to 0.55, occurring at a rain rate of about 2 mm hr^{-1} and reflectivity of 29 dBZ.

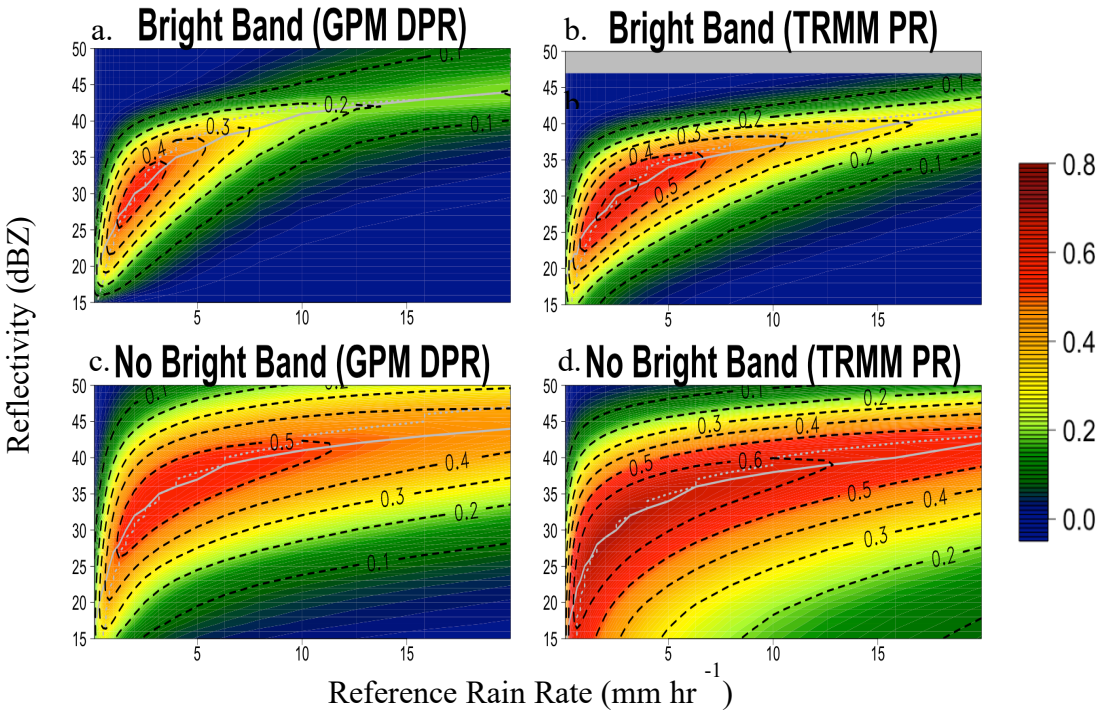

Figure 15: 2D-HSS bivariate histograms the GPM-DPR (left) and TRMM-PR (right) for cases when the bright band is (top) and is not (bottom) detected.

Figure 8b is the TRMM-PR. Like the GPM-DPR, the areal extent of the scores associated with some delineation skill decreases significantly, although at higher rain rates the scores do not decrease as quickly as they do with the GPM-DPR. Also similar to the GPM-DPR, the area of the scores greater than 0.6 is much less than the general performance, and the scores associated with precipitation detection (i.e., the minimum detectable signal) are much smaller, decreasing from greater than 0.6 in the general performance to near 0.2 when the bright band is detected. The maximum score greatly decreases to 0.62, occurring at a rain rate of 2.51 mm hr^{-1} and reflectivity of 29 dBZ.

3.6.2 No Bright Band

Figure 8c is the 2D-HSS for the GPM-DPR when bright band is not detected. The area of positive scores is slightly larger than the general performance of the radar. Scores are slightly higher at

lower rain rates and higher reflectivity values, but about the same at high reflectivity values and high rain rates, although scores are slightly higher at lower reflectivity values at the high rain rates. The scores that are greater than 0.5 reaches further into the high rain rates, extending past 10 mm hr^{-1}. While the scores greater than 0.5 do not go as far into the lesser reflectivity values at lower rain rates, the scores do not decrease as quickly as the general performance as the reflectivity values decrease, leading to a greater score near the minimum detectable signal of the instrument when no bright band is detected. The maximum overall score is the same, 0.56, but occurring at a higher reflectivity and rain rate of 34 dBZ and 3.16 mm hr^{-1}, respectively.

Figure 8d is for the TRMM-PR. Compared to the general performance of the TRMM-PR, the distribution of scores is very similar. The differences are seen most easily in the area of scores greater than 0.6. Near 38 dBZ, for example, this area is extended from a rain rate of about 10 mm hr^{-1} in the general performance to about 12.5 mm hr^{-1} when no bright band is detected. At lower rain rates, such as at about 1 mm hr^{-1}, however, the coverage of this area decreases from less than 15 dBZ in the general performance to about 17 dBZ when no bright band is detected. The maximum score is slightly less as well, at 0.69, occurring at a rain rate of about 2 mm hr^{-1} and reflectivity of 28 dBZ.

3.7 Shallow Rain

Figure 9 is the 2D-HSS histogram for the GPM-DPR and TRMM-PR for cases with no shallow rain and cases with shallow rain. Shallow rain occurs in the lowest portions of the atmosphere, where a spaceborne radar can have contamination due to backscattering from the surface, which could affect the ability of the radar to not only delineate, but also detect shallow precipitation. Note, the TRMM-PR data does not have a variable specifically for shallow rain, but does for warm rain, and is used as an estimate for shallow rain.

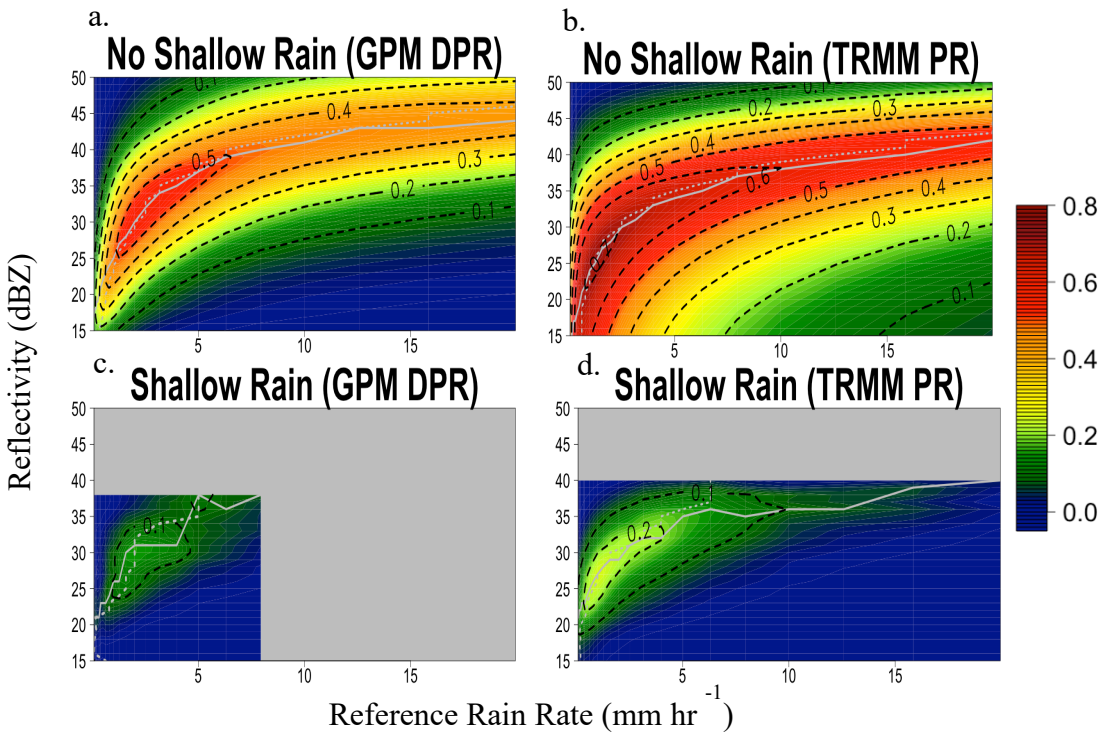

Figure 17: 2D-HSS bivariate histograms for GPM-DPR (left) and TRMM-PR (right) for cases without (top) and with (bottom) shallow rain.

3.7.1 No Shallow Rain

Figure 9a depicts the 2D-HSS for the GPM-DPR in cases with no shallow rain. There is very little difference between cases without shallow rain and the general performance of the radar. In fact, it reaches the same maximum score of 0.56 at the same rain rate of 2.51 mm hr^{-1} and reflectivity of 31 dBZ.

Figure 9b is for the TRMM-PR. Similar to the GPM-DPR, the distribution of scores is very similar to the general performance, with some differences to note. While the distribution of scores across reflectivity values is very similar, the distribution across rain rates is slightly improved. For example, the 0.1 contour goes from about 13 mm hr^{-1} in the general performance to about 15 mm hr^{-1} in cases without shallow rain. The area of scores greater than 0.6 is also slightly expanded

in this way. One other difference to note is the addition of an area of scores greater than 0.7. The maximum score of 0.71 occurs at a rain rate of about 1.25 mm hr^{-1} and reflectivity of 24 dBZ.

3.7.2 Shallow Rain Only

Figure 9c is the 2D-HSS for the GPM-DPR with shallow rain. Note that, while the sample size is significantly smaller, the distribution of scores in areas with sufficient sample size is greatly different than the general performance of the radar. Scores near the minimum detectable signal of the radar are very near zero, and all scores within the area do not exceed 0.2. The maximum score is 0.16, achieved at a reflectivity of 30 dBZ and rain rate of about 2 mm hr^{-1}.

Figure 9d is for the TRMM-PR. Similar to the GPM-DPR, the distribution of scores is significantly smaller when compared to the general performance of the radar. Most scores do not exceed 0.2, and the maximum score is only 0.25, occurring at a reflectivity of 26 dBZ and rain rate of 1 mm hr^{-1}.

4 Discussion

4.1 Comparison of General Performance of Each Radar

The distribution of HSS scores for the TRMM-PR and GPM-DPR shows that they both have delineation capabilities over a wide range of rainfall rates and reflectivity conditions. The GPM-KuPR has delineation capabilities over a lesser range of rainfall rates and reflectivity conditions, performing the best at lower rainfall rates. Decreasing values of HSS with increasing rain rates highlight the challenge of delineating high rain rates that are predominantly associated with convection and attenuated radar signal. Figure 10 depicts the difference between each radar, both overall and when coastal surfaces and midlatitudes are excluded.

4.1.1 TRMM-PR GPM-DPR Comparison

The distribution of scores for the GPM-DPR indicates that it has delineation capabilities over a similar range of rainfall rates and reflectivity conditions compared to the TRMM-PR. The GPM-DPR performs slightly better than the TRMM-PR at higher reflectivity values (greater than about 40 dBZ) across all rain rates. For both radars, the range of reflectivity thresholds associated with some delineation skill (i.e., positive HSS scores) is maintained at larger rain rate thresholds. Focusing on conditions that maximize the delineation capabilities (HSS greater than 0.5), the TRMM-PR displays better performance at almost all reflectivity values across all rain rates, as indicated by the orange and red areas in figures 3a and b. The GPM-DPR shows significantly lower delineation capabilities for rain rates lower than 2 mm hr^{-1}, and reflectivity lower than 25 dBZ, indicating that the TRMM-PR performs better in the detection of precipitation.

Figure 10a shows the difference in scores between the TRMM-PR and GPM-DPR. Positive values indicate that the GPM-DPR performs better. The GPM-DPR performs better across almost

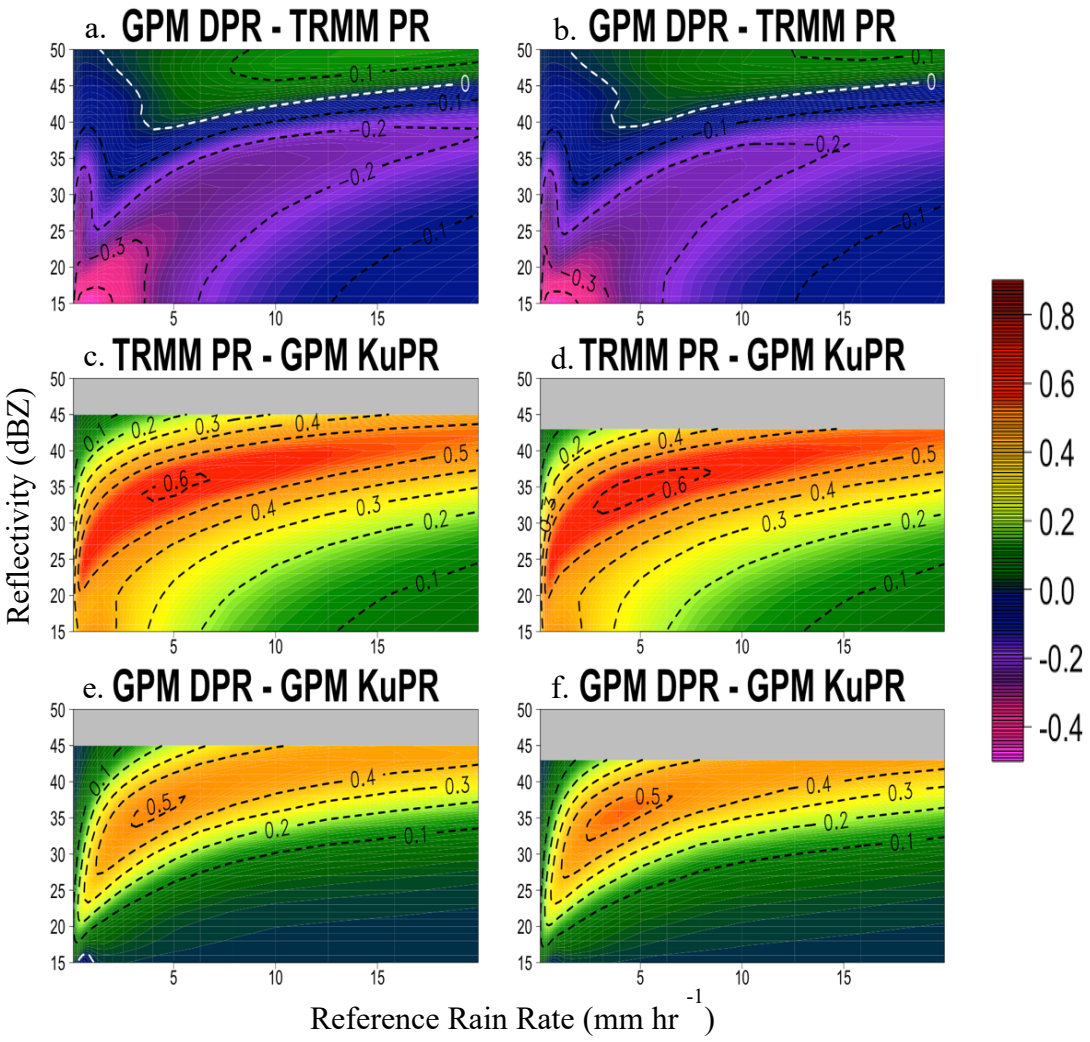

Figure 19: Differences in delineation skill between the (a) GPM-DPR and TRMM-PR, (c) TRMM-PR and GPM-KuPR, and (e) GPM-DPR and GPM-KuPR. (b), (d), and (f) are the same as (a), (c), and (e), respectively, with coastal surfaces and latitudes greater than 37° excluded.

all rain rates when the reflectivity is greater than about 40 dBZ. The TRMM-PR, however, performs better at lower reflectivity values, and especially at lower reflectivity values and rain rates. A similar result is seen when the TRMM-PR is compared to the GPM-DPR with no coastal areas and in the tropics (figure 10b).

4.1.2 Comparisons with GPM-KuPR

The score distribution for the GPM-KuPR indicates that it has delineation skill over a much smaller range of rain rates and reflectivity values. Additionally, the overall delineation capabilities of the GPM-KuPR are much less than the two previous radars, with only low to moderate skill. The GPM-KuPR decreases to nearly 0 with increasing rain rate, while the other radars maintain at least some skill.

Figure 10c shows the difference in scores between the TRMM-PR and GPM-KuPR, while figure 10e has the difference between the GPM-DPR and GPM-KuPR. Both the TRMM-PR and GPM-DPR perform better than the GPM-KuPR across almost all rain rates and reflectivity values, although the TRMM-PR performs better to a greater extent. The TRMM-PR also performs better than the GPM-KuPR at low rain rates and reflectivity, whereas the GPM-DPR and GPM-KuPR perform much more similarly in this area. Again, the differences in skill remain similar when coastal surfaces and the midlatitudes are excluded (figures 10d and f).

4.1.3 Overall Comparison

Overall, all the radars have a similar shape and HSS pattern (figure 3). Their delineation skills are more sensitive to changes in precipitation rates at lower rainfall magnitudes and more sensitive to changes in reflectivity at higher rainfall magnitudes. The HSS is generally higher for moderate reference rain rates and reflectivity. Looking across the missions, neither the GPM-DPR nor the GPM-KuPR reach as high of skill as the TRMM-PR. One possible explanation of this is that the signal processing is affected by the noise level. Despite lower scores elsewhere, the GPM-DPR has the greatest delineation skill across almost all reference rain rates at high reflectivity, while the TRMM-PR has the best skill at lower reflectivity.

4.2 Precipitation Classification

Figure 11 depicts the difference in scores between stratiform and convective cases. Areas where the values are positive indicate that stratiform cases yielded higher scores, while negative values are associated with convective instances having higher score. Figure 12 has the difference in scores between the general performance of the radar and the specific precipitation classification. Note, comparisons will now be between the different instances on the same radar, and how each radar did compared to the general performance.

4.2.1 Stratiform Versus Convective

Figure 11a shows the difference in scores for the GPM-DPR, while figure 11b is for the TRMM-PR. As expected, both radars performed better at lighter rain rates in cases of stratiform and better at higher precipitation rates in the convective precipitation instances. At lower rain rates, stratiform performs better than convective. The precipitation pixels go through different algorithms depending on if they are flagged as either stratiform or convective. Additionally, convective precipitation is associated with higher variability (nonuniformity) within the footprint and is more challenging to quantify compared to stratiform precipitation. It is interesting to note that while the radars performed better at lower rain rates and reflectivity values in cases with stratiform, it was only an improvement of about 0.1 compared to convective cases, while at the higher rain rates and reflectivity, convective cases yielded improvements in scores by 0.2 to 0.3.

4.2.2 Overall Effect

Figure 12a illustrates the difference between the overall performance of the GPM-DPR and cases of stratiform precipitation. The two perform very similarly at lower rain rates, while the overall

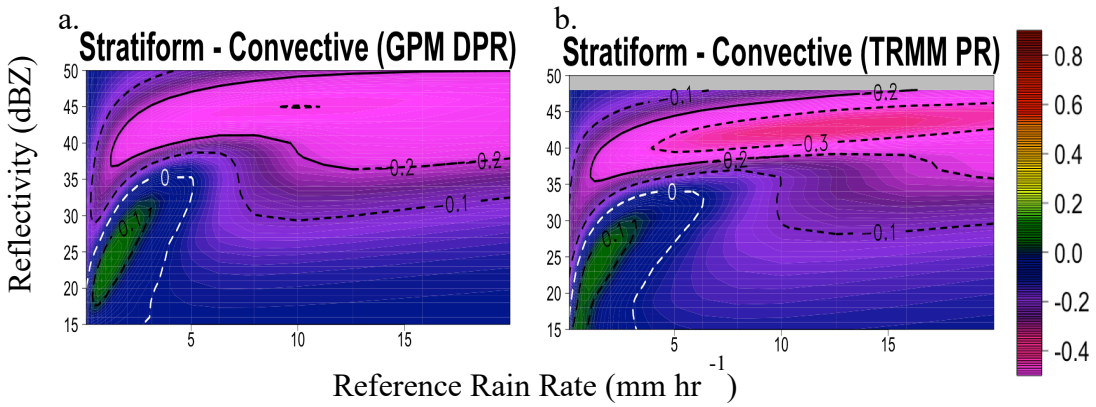

Figure 21:Difference in HSS between instances with only stratiform precipitation and only convective precipitation for the GPM-DPR (a) and TRMM-PR (b).

performance of the GPM-DPR is better at higher rain rates. This is to be expected, as stratiform precipitation is associated with lower rain rates.

Figure 12b has the difference in scores between the TRMM-PR overall performance and stratiform cases. Unlike the GPM-DPR, the overall performance of the TRMM-PR yields higher scores everywhere, although the scores are closer at lighter rain rates, with differences of only 0.1 to 0.2, compared to higher rain rates, where differences in scores exceed 0.3. The differences for both radars suggest that stratiform precipitation can have a negative effect on delineation of higher precipitation rates and reflectivity values. The sample sizes at these areas of higher values, however, are small and might mitigate the impact on the overall score.

Figure 12c is the difference between the GPM-DPR overall performance and convective cases. Again, as expected, both perform similar to each other at higher rain rates, while the overall performance is better at lower rain rates. Interestingly, instances of convective precipitation yield a slightly higher score at lower rain rates and higher reflectivity values. This could be due to a negative impact from some other variable, such as the presence of the bright band or land type.

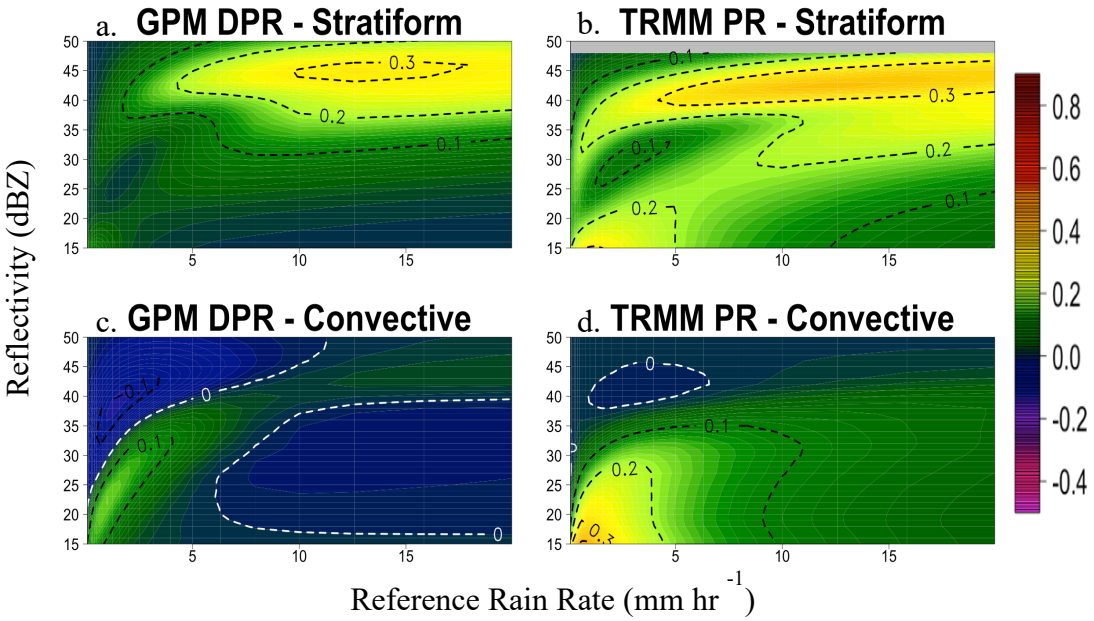

Figure 23: Differences in HSS between the overall performance for the GPM-DPR (left) and TRMM-PR (right) and the cases with just stratiform precipitation (top) and convective precipitation (bottom).

Figure 12d illustrates the difference between the TRMM-PR overall skill and skill in cases of convective precipitation. The comparison of these yields a result similar to the convective cases with the GPM-DPR. The TRMM-PR has much higher capabilities in detecting precipitation when focusing on all cases, compared to when the cases are just convective, seen in the positive scores exceeding 0.3 at very low rain rates and low reflectivity. However, the TRMM-PR performs very similarly at higher rain rates in instances with convection and overall.

The differences with convective cases suggest that convective precipitation significantly decreases the precipitation detection skill of the TRMM-PR and delineation at lower rain rates and reflectivity values for both radars. The sample sizes in this area are also larger than the sample sizes of stratiform cases at higher rain rates and reflectivity, suggesting that the overall skills (as well as maximum skills) are affected more by convective precipitation than stratiform precipitation.

4.3 Regional Differences

Figure 13 is the difference in scores for the GPM-DPR between the tropics and midlatitudes. Areas with positive values indicate that the GPM-DPR performed better in the tropics, where negative values mean that it performed better in the midlatitudes. Figure 14 is the difference between the GPM-DPR skill overall and the skill in both the tropics and midlatitudes.

4.3.1 Tropics Versus Midlatitudes

From figure 13, the GPM-DPR performs slightly better in the tropics in almost all instances. Surprisingly, the GPM-DPR performs slightly better in the midlatitudes at higher reflectivity values across most rain rates. Since the tropics typically has more convection than the midlatitudes, and instances of convective precipitation yielded better performance at these higher reflectivity values across all rain rates (figures 4 and 11), it would be expected that the GPM-DPR would have better performance in the tropics in this area. Note that the difference in scores across all reference rain rates and reflectivity values, however, is rather small (less than 0.1), especially when compared to some of the differences in the scores found in comparing convective and stratiform or comparing the overall skill of the radars to one another, suggesting that differences in skill due to region are not as significant as other factors.

4.3.2 Overall Effect

Figure 14a illustrates the difference in scores between the overall skill of the GPM-DPR and its performance in the tropics. Expectedly, their performances are very similar across most rain rates and reflectivity values, while the GPM-DPR overall skill is slightly greater at those same reflectivity values and rain rates in which the GPM-DPR performed better in the midlatitudes.

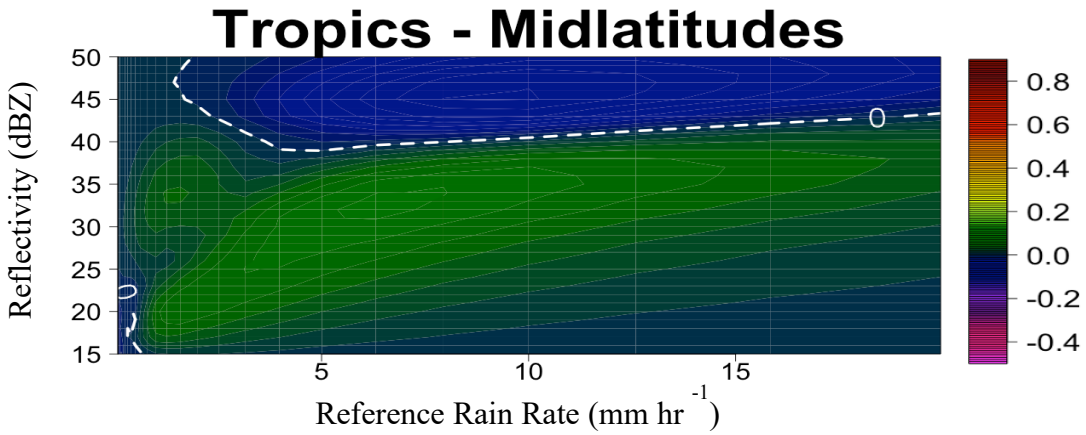

Figure 25: Difference in HSS for the GPM-DPR between the tropics and midlatitudes.

Figure 14b depicts difference in the overall skill and the skill in the midlatitudes. Again, as expected, the two perform similarly at the higher reflectivity values across most rain rates, while the GPM-DPR overall performs slightly better elsewhere. Like the difference between the scores in the tropics and midlatitudes, the difference overall between the overall skill and both the skill in the tropics and midlatitudes is small, not significantly affecting the overall skill.

4.4 Effect of Zenith Angle

Figure 15 is the difference in HSS between Near and Far nadir angles. Positive (negative) values indicate that data with near (far) nadir angles performed better than far (near) nadir angles. Figure 16 depicts the difference in skill between the general performance of the radars and when measurements are taken at near and far nadir angles.

4.4.1 Near Versus Far Nadir

From figure 15, measurements taken at angles near the nadir point performed slightly better than measurements taken at angles far from the nadir point across almost all reflectivity values and rain rates. This is to be expected, as a common assumption with the algorithms is that the radar beam is vertical. Additionally, non-uniform beam filling is more prevalent at far nadir angles. One

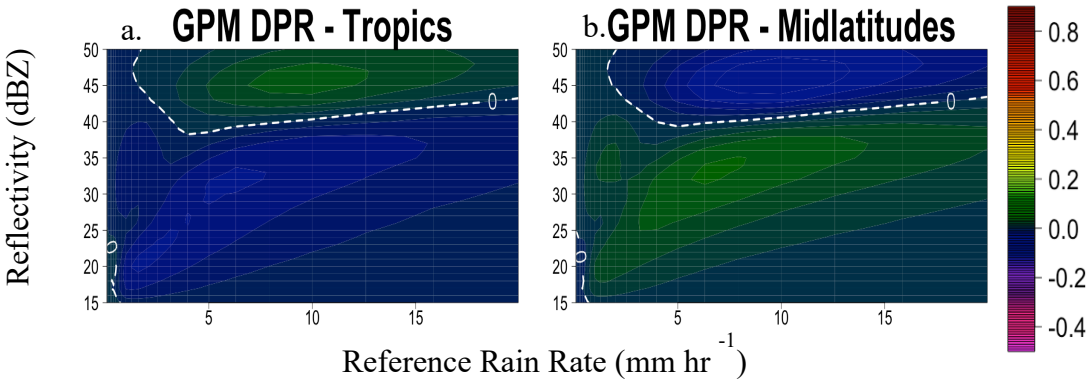

Figure 27: Difference in skill scores for the GPM-DPR overall skill and its skill in the tropics (a) and midlatitudes (b).

noticeable exception with the GPM-DPR is when reflectivity values are near 40 dBZ and rain rates are greater than about 6 mm hr^{-1}. The scores yielded from far nadir angles in this area, however, are only slightly higher than those yielded from near nadir angles, with an increase in score of only about 0.03 to 0.04. The scores yielded from near nadir angles are much greater than the scores from far nadir angles at higher reflectivity values, and especially at higher reflectivity values and high rain rates, where the score at near nadir angles is almost 0.1 greater than the scores at far nadir angles for the GPM-DPR, and .13 to .14 for the TRMM-PR.

4.4.2 Overall Effect

Figure 16a is the difference in skill scores between the general performance of the GPM-DPR and when measurements are taken at near nadir angles, while figure16b is for the TMM-PR. Overall, for both radars, the measurements taken at near nadir angles perform slightly better than the general performance. Again, this is to be expected, as many algorithms assume that measurements are taken at the nadir point. The GPM-DPR performs slightly better (an improvement in score of only 0.01 to 0.02) near 40 dBZ and at rain rates greater than 10 mm hr^{-1}, while the TRMM-PR performs

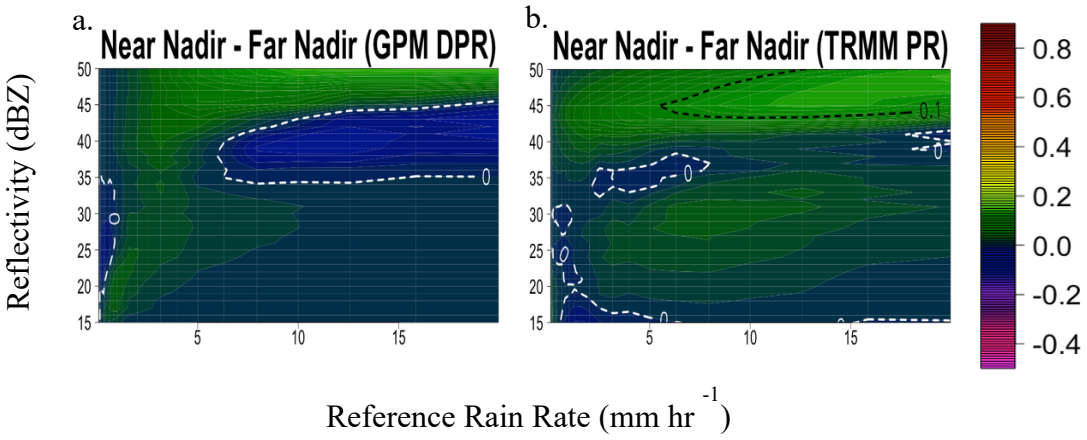

Figure 29: Difference in HSS between near nadir and far nadir angles for the GPM-DPR (a) and TRMM-PR (b).

slightly better (although only an improvement of less than 0.01) between 35 and 40 dBZ at rain rates higher than about 5 mm hr^{-1}.

Figures 16c and d show the difference in skill between the general performance and far nadir angles. The overall performances for both the GPM-DPR and TRMM-PR yield higher scores in most cases. This is to be expected, as far nadir angles would break the assumption of a vertical beam the most and yield lower scores. For the GPM-DPR, much like in the comparison with near nadir angles, however, the far nadir angles yield a higher score near 35 dBZ at rain rates greater than about 4 mm hr^{-1}, although the difference in scores is only 0.03 to 0.04. Overall, for both radars and both near and far nadir angles, the differences in scores are less than 0.1, so zenith angle does not have a significant impact.

4.5 Differences due to Surface Type

Figure 17 depicts the differences in the HSS for different surface types for the GPM-DPR and the TRMM-PR. Figure 18 is the difference in the HSS between the general performances and the different surface types for the GPM-DPR and TRMM-PR. Positive values indicate that the general

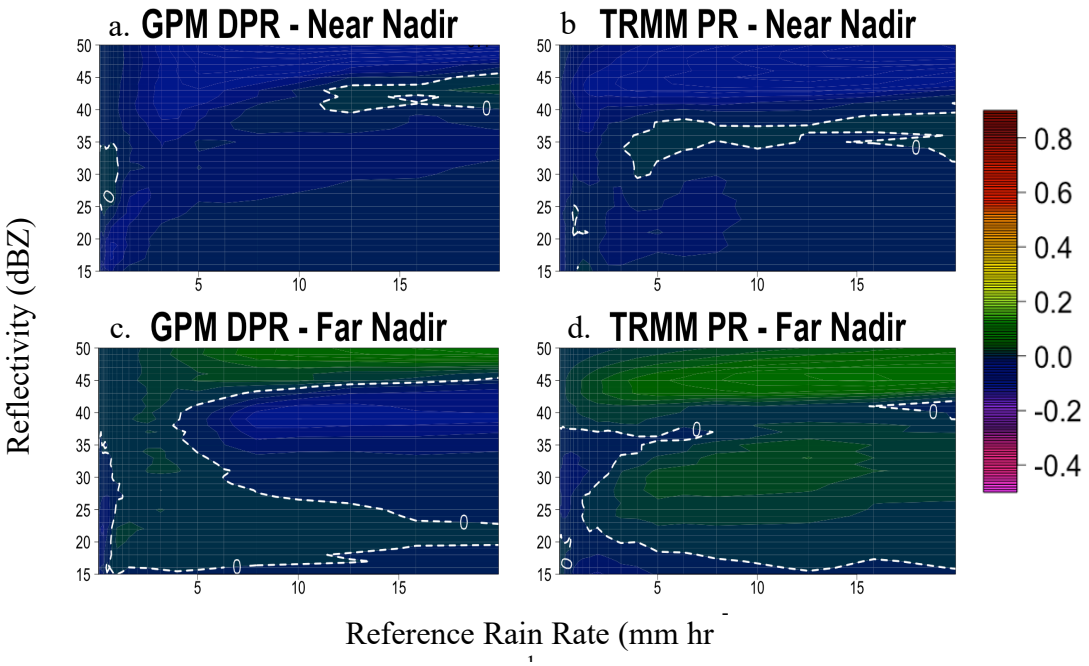

Figure 31: Difference is skill score between the GPM-DPR (left) and TRMM-PR (right) general performances and near (top) and far (bottom) nadir angles.

performance yielded higher scores, while negative values mean that the score was higher for the specific surface type.

4.5.1 Comparing Surface Types

Figures 17a and b are the score differences between the land and ocean surface types for the GPM-DPR and TRMM-PR, respectively. For both radars, the land surface type yields a higher score across all reflectivity values at very low rain rates (less than about 1 mm hr^{-1}) and across all rain rates at reflectivity values greater than 42 dBZ for the GPM-DPR and 37 dBZ for the TRMM-PR. The TRMM-PR, however, also yields higher scores for the land surface type across most reflectivity values when the rain rate is above about 8 mm hr^{-1}. Focusing on the GPM-DPR, the land surface type has an improvement in score of almost 0.2 at very low rain rates and reflectivity around 25 dBZ. For the TRMM-PR, the land surface is greater than the ocean surface by more

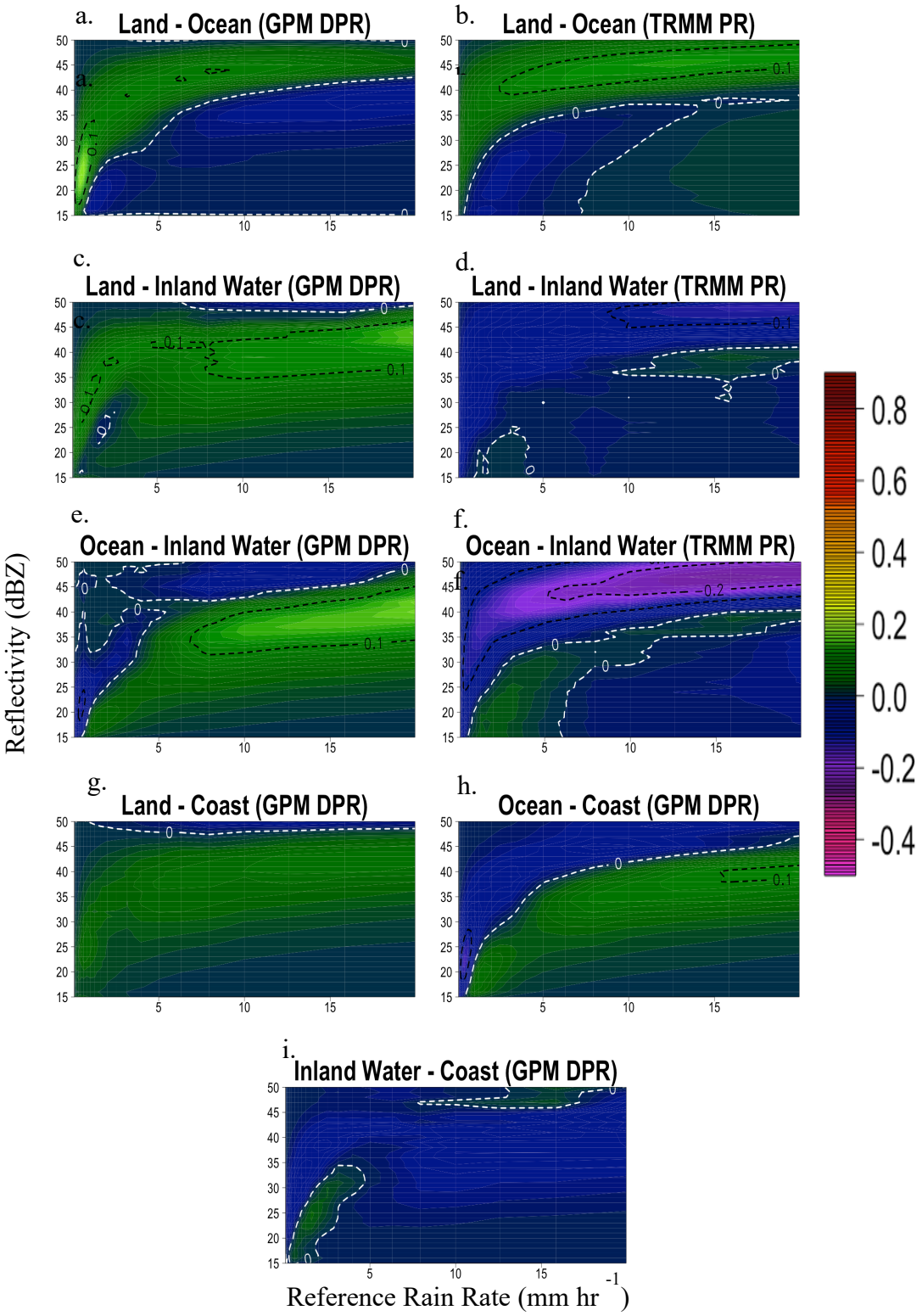

Figure 33: Differences in HSS between different surface types. (a), (c), (e), (g), (h), and (i) are for the GPM-DPR, while (b), (d), and (f) are for the TRMM-PR.

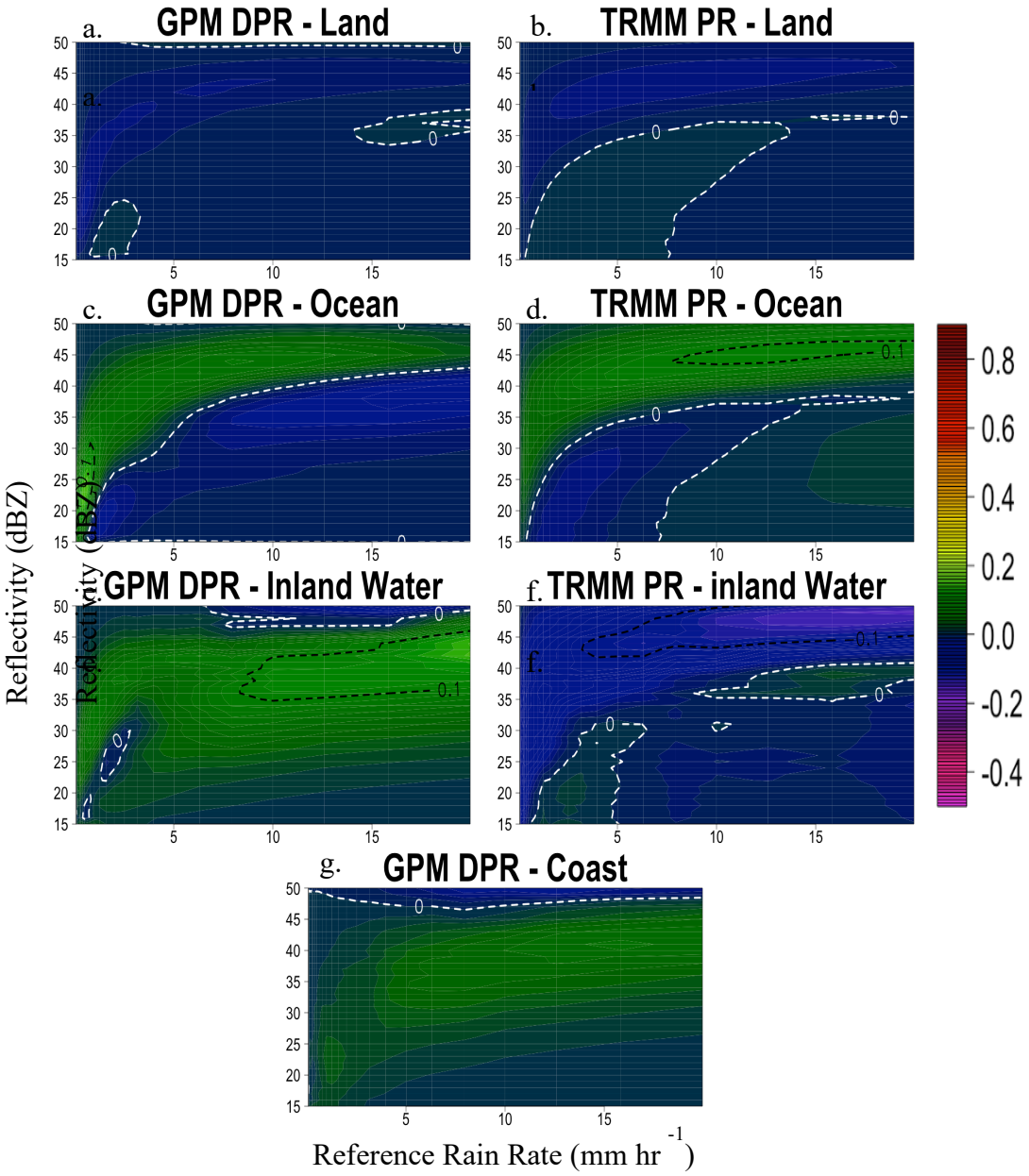

Figure 35: Difference in skill score between the general performance and the land (a), ocean (c), inland water (e), and coast (g) surface types for the GPM-DPR. (b), (d), and (e) are the same as (a), (c), and (e) but for the TRMM-PR.

than 0.1 across higher reflectivity values and rain rates greater about 3 mm hr^{-1}. For both radars, when the ocean surface type performs better, it is only by about 0.04.

Figure 17c depicts the difference in skill between the land and inland water surfaces for the GPM-DPR. The land surface type yields a higher score across almost all reflectivity values and rain rates, although the scores are more similar to each other at very high reflectivity values and near a reflectivity of 25 dBZ and rain rate of about 2.5 mm hr^{-1}. Figure 17d is for the TRMM-PR. Unlike the GPM-DPR, the inland water surface yields higher scores across almost all reflectivity values and rain rates. The land surface type does yield higher scores around a reflectivity of 37 dBZ and rain rates greater than 10 mm hr^{-1}.

Figure 17e (17f) is the difference between the ocean and inland water surface type for the GPM-DPR (TRMM-PR). Focusing on the GPM-DPR, the ocean surface performs better across most reflectivity values and rain rates. The inland water surface, however, performs slightly better at reflectivity values greater than about 45 dBZ and rain rates greater than about 4 mm hr^{-1}, as well as at lower reflectivity values and lower rain rates, exceeding an improvement of over 0.1 near the nominative sensitivity of the instrument, between 18 and 25 dBZ for a rain rate of about 0.5 mm hr^{-1}. The ocean yields its highest difference in score at moderate reflectivity values across higher rain rates, where the difference in score also exceeds 0.1.

Shifting to the TRMM-PR, the inland water yields higher skill across almost all reflectivity values and rain rates, exceeding an improvement in score of over 0.2 at higher reflectivity and rain rates. The ocean, however, does yield slightly higher scores, although the difference is less than 0.1, at rain rates lower than about 5 mm hr^{-1} and reflectivity less than about 30 dBZ, and extending into higher rain rates at a reflectivity of about 37 dBZ.

Figures 17g, h, and i depict the difference in skill between the land, ocean, and inland water surface types and the coast surface type for the GPM-DPR. Focusing on the land coast difference, the land type yields higher scores across all rain rates for reflectivity less than about 43 dBZ, while

the coast type yields slightly higher scores at the very high reflectivity values. These differences in scores, however, are both less than 0.1.

Shifting to ocean coast difference, the ocean surface type yields higher scores across almost all rain rates at lower reflectivity and higher rain rates at higher reflectivity, exceeding a difference in score of 0.1 around 40 dBZ when rain rates are higher than about 15 mm hr^{-1}. The coast yields a higher skill across almost rain rates at higher reflectivity and across almost all reflectivity values at lower rain rates. It outperforms the ocean type by more than 0.1 at rain rates less than about 0.5 mm hr^{-1} at reflectivity values near about 23 dBZ.

Looking at the inland water coast difference, the coast surface type yields a slightly higher reflectivity across almost all rain rates and reflectivity. The inland water performs slightly better at lower rain rates and reflectivity values, as well as at very high reflectivity and high rain rates. Like the land coast difference, none of the score differences exceed 0.1.

4.5.2 Overall Effect

Figure 18a shows the difference in score between the general performance of the GPM-DPR and the land surface type. Overall, they perform very similarly to each other, with the largest difference not exceeding 0.04, but the land surface does perform slightly better across almost all reflectivity and rain rates, with them performing more similarly at very high reflectivity, at rain rates greater than 15 mm hr^{-1} and reflectivity around 35 dBZ, and lower reflectivity and rain rates.

Figure 18b is for the TRMM-PR. Like the GPM-DPR, the land surface type performs slightly better (again differences do not exceed 0.04) across almost all rain rates and reflectivity. The general performance and land surface types perform very similarly at rain rates less than about 8 mm hr^{-1} and reflectivity less than about 35 dBZ, extending to higher rain rates at about 37 dBZ.

Figures 18c and d are the difference between the general performance and ocean surface type for both radars. The general performance yields higher scores with both radars at all reflectivity values at the lowest rain rates and at higher reflectivity values as rain rate increases. The general performance of the GPM-DPR has an improvement over the ocean surface type of over 0.1 at very low rain rates and reflectivity between about 18 and 30 dBZ, while the general performance of the TRMM-PR outperforms the ocean surface by greater than 0.1 at higher reflectivity across higher rain rates. The TRMM-PR general performance also is more skilled than the ocean surface across the lower reflectivity values at higher rain rates. For both radars, although the rest of the area is where the ocean yields higher scores, it does not exceed improvements of 0.05 for the GPM-DPR and 0.03 for the TRMM-PR. This suggests that the ocean surface type has a negative impact on the skill. The ocean surface type, however, effects the overall score for the GPM-DPR more than for the TRMM-PR due to sample size.

Figure 18e is the difference in skill score between the general performance of the GPM-DPR and the inland water surface type. The general performance yields higher scores across almost all reflectivity values and rain rates, with the difference exceeding 0.1 at moderate to high reflectivity values at higher rain rates. The inland water surface performs slightly better than the general performance at the highest reflectivity values and high rain rates, as well as at lower reflectivity and rain rates, although this difference does not exceed about 0.03.

Figure 18f is for the TRMM-PR. Unlike the GPM-DPR, the inland water performs better than the general performance across most reflectivity values and rain rates, with the difference exceeding 0.1 at higher reflectivity values across moderate to high rain rates. The general performance is slightly better at lower reflectivity and rain rates, as well around 38 dBZ at rain rates greater than 10 mm hr^{-1}, but the difference in scores is not greater than 0.03. The differences

for both radars suggest that the inland water type has a negative effect on the GPM-DPR, but a positive one on the TRMM-PR. Again, however, due to a small sample size, its impact is reduced on the overall skill for both radars.

Figure 18g is the HSS difference between the general performance of the GPM-DPR and the coast land type. The general performance is better than the coast land type across almost all reflectivity and rain rates, with an exception at the highest of reflectivity. The differences in the scores, however, are not greater than 0.1.

4.6 Bright Band

Figure 19 is the difference in skill scores between when bright band is detected by the spaceborne radars and when it is. Positive scores indicate that higher scores are yielded in cases with the bright band present, while negative scores mean that cases with no bright band yield higher scores. Figure 20 shows the difference between the general performance of the radars and when bright band either is or is not detected.

4.6.1 Comparing bright band to no bright band

Figure 19a shows the difference in skill between bright band and no bright band for the GPM-DPR, while figure 19b is for the TRMM-PR. Focusing on the GPM-DPR, cases without the bright band yield higher scores. In particular, cases with no bright band yield much higher scores at very low rain rates and reflectivity values. This means that the bright band impacts the accuracy of precipitation detection, and that the detection of precipitation is less accurate when the bright band is detected/present. Cases where no bright band is detected also yields a much higher score across almost all rain rates at higher reflectivity, suggesting that the presence of the bright band has a negative impact on the delineation of heavier precipitation. There is a small area near reflectivity

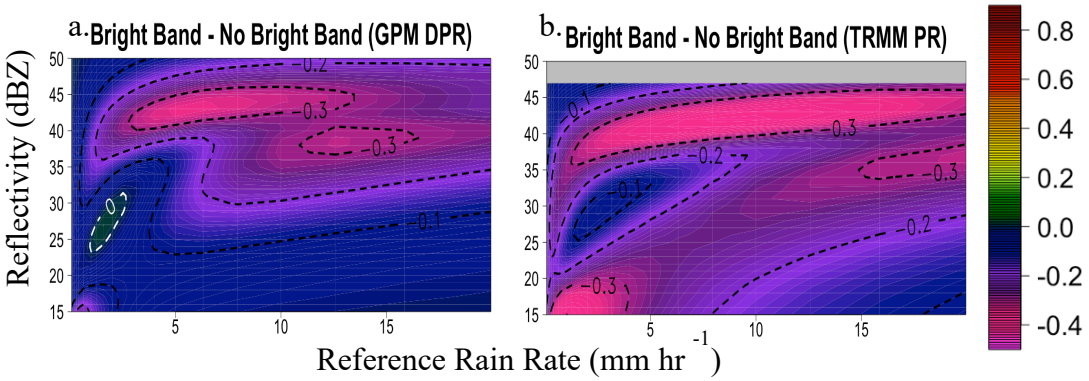

Figure 37: Difference in HSS between when bright band is detected and when it is not detected for the GPM-DPR (a) and TRMM-PR (b).

values of 27 dBZ and rain rates of 2 mm hr^{-1} where the differences in the score are much more similar to each other, with cases with the bright band performing slightly better, although the difference is less than 0.02. Shifting to the TRMM-PR, cases without the bright band yield higher scores across all reflectivity values and rain rates. Like the GPM-DPR, the areas where this difference is the greatest is at low reflectivity values and low rain rates, as well as across all rain rates at higher reflectivity.

4.6.2 Overall Effect

Figures 20a and b show the difference in the HSS between the general performance of the GPM-DPR and TRMM-PR, respectively, and cases with no bright band for each radar. For both radars, cases with no bright band detected yield slightly higher scores, with differences in the scores exceeding 0.1 at high reflectivity values and low rain rates as well as reflectivity near 35 dBZ and rain rates between 10 and 15 mm hr^{-1} for the GPM-DPR. The general performances of the radars yield slightly higher scores, however, at reflectivity values near 30 dBZ and rain rates near 2 mm hr^{-1}, with this area extending to lower rain rates and reflectivity for the TRMM-PR. This implies

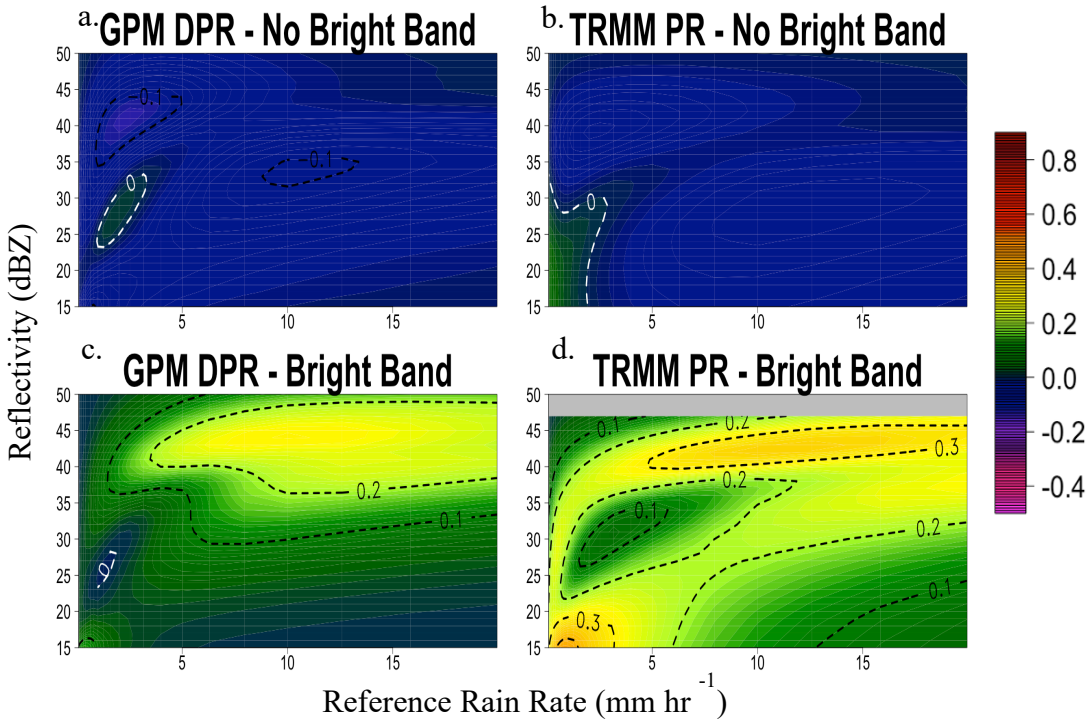

Figure 39: Difference in skill score between general performances of the GPM-DPR (left) and TRMM-PR (right) and cases when the bright band is (top) and is not (bottom) detected.

that the detection of precipitation is slightly more accurate when no bright band is detected for the GPM-DPR, but not for the TRMM-PR.

Figure 20c and d are cases when bright band is detected. For both radars, their general performances yield higher scores almost everywhere for the GPM-DPR and everywhere for the TRMM-PR. The general performances yield notably higher scores at lower rain rates and reflectivity values, as well as at higher reflectivity values across all rain rates. There is a small area for the GPM-DPR at which cases with bright band yield slightly higher scores at a reflectivity near 27 dBZ and rain rate near 2 mm hr^{-1}, but this difference is less than 0.01. Again, the differences at high reflectivity values suggest that bright band negatively effects the skill, but sample size is small enough to limit its impact. For the TRMM-PR, however, the area of differences at very low rain

rates and reflectivity values has a larger sample size, suggesting that the presence of the bright band has a significant negative impact on the detection of precipitation.

4.7 Shallow Rain

Figure 21 depicts the difference in skill scores between cases with no shallow rain and cases with shallow rain for the GPM-DPR and TRMM-PR. Figure 22 shows the overall difference between the general performances of each radar and cases with and without shallow rain.

4.7.1 No Shallow Rain Versus Shallow Rain

Figure 21a depicts the difference in HSS for the GPM-DPR between cases with no shallow rain and cases with shallow rain. Cases without shallow rain yield higher scores across all the rain rates and reflectivity values that have sufficient sample size. It yields significantly higher scores at moderate reflectivity and rain rate (around 35 dBZ and 5 mm hr^{-1}, respectively).

Figure 21b is for the TRMM-PR. Like the GPM-DPR, cases without shallow rain yield higher scores across all rain rates and reflectivity values. There are two areas of significant difference, at low reflectivity and rain rate, where the difference in the scores exceeds 0.6, as well as at higher reflectivity values at higher rain rates, where the difference exceeds 0.5. The differences for both radars suggest that shallow rain has a significant impact on skill and highlight the issue of the spaceborne radars' blind spot in the lower part of the atmosphere due to contamination of backscattering from the surface and the challenges of both detecting and delineating precipitation magnitudes when shallow rain is present.

4.7.2 Overall Effect

Figures 22a and b have the difference in scores between the general performance of the GPM-DPR and TRMM-PR, respectively, and cases with no shallow rain. It was stated in the results that there

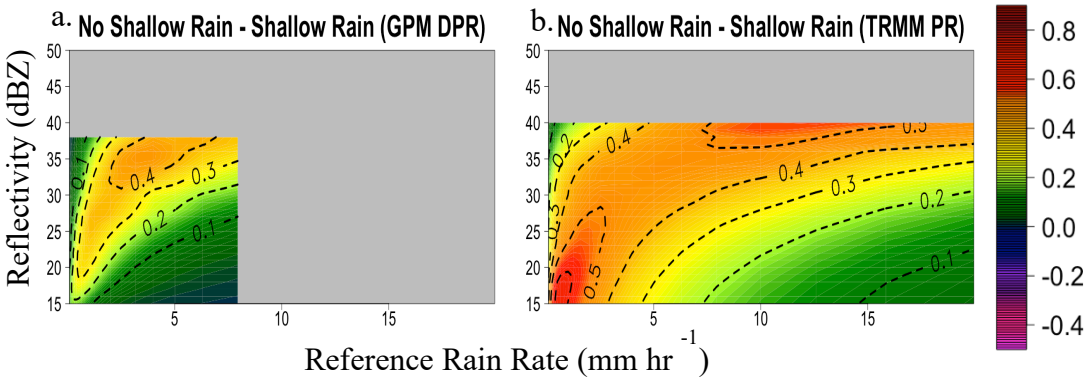

Figure 41: Difference in HSS between cases without and with shallow rain for the GPM-DPR (a) and TRMM-PR (b).

was very little difference between the general performance of both radars and the cases with no shallow rain. These figures confirm this statement.

With the GPM-DPR, the cases with no shallow rain yield slightly higher scores in most areas, with the exception of at higher reflectivity values at the lightest of rain rates and at reflectivity values near 37 dBZ at higher rain rates, but across all rain rates and reflectivity values, the difference in scores does not exceed 0.01. Focusing on the TRMM-PR, across most rain rates and reflectivity values, there is very little difference (the cases with no shallow rain perform better, but with a difference in scores of less than 0.01). At lower reflectivity and rain rates, the cases with no shallow rain perform slightly better, but the difference is less than 0.04.

Figures 22c and d are the differences in scores between the general performance of each radar and cases with shallow rain. Given that the differences between the general performance and cases with no shallow rain for both radars are very small, this difference histograms look very similar to the difference between cases without and with shallow rain. The general performances yield much higher scores than the cases with shallow rain. This implies that shallow rain has a significant negative impact on the precipitation delineation capabilities of both radars. However, due to a very small sample size (about 6500 cases compared to about 700000 cases in the general performance

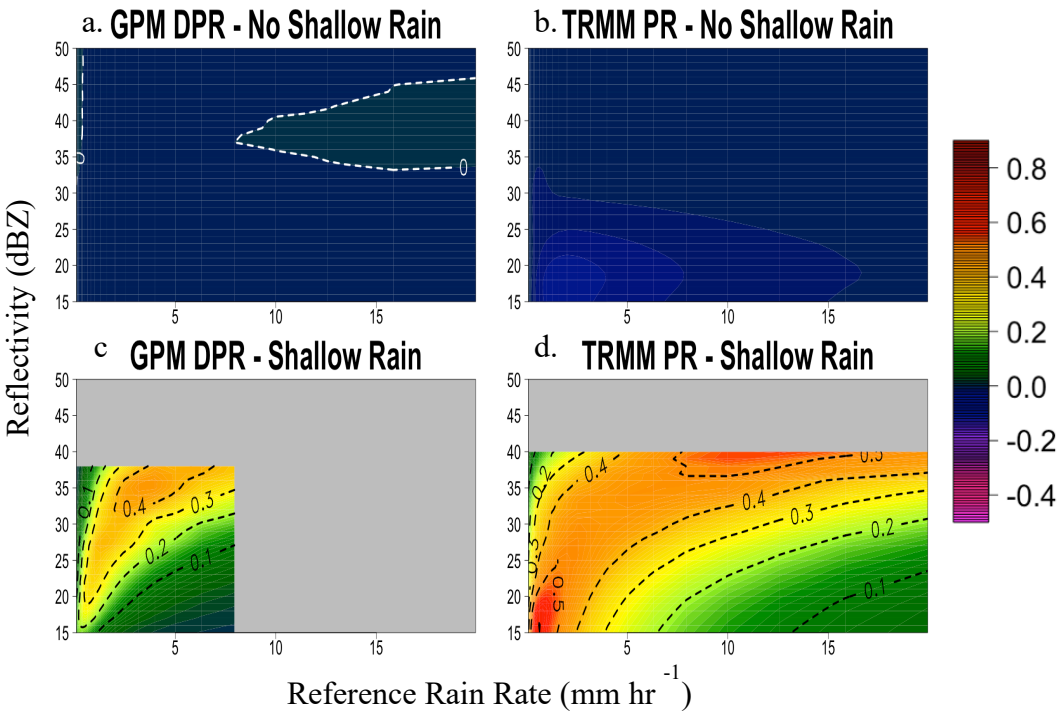

Figure 43: Differences in skill score between the general performances of the GPM-DPR (left) and TRMM-PR (right) and cases without (top) and with (bottom) shallow rain.

for the GPM-DPR, and about 45000 cases compared to 1.5 million cases for the TRMM-PR), its overall impact is small.

5 Conclusion

Water is crucial to every living thing on Earth. Understanding how it is transported throughout the water and energy cycles, and how it is distributed in a changing climate requires knowledge of when, where, and how much precipitation is falling at a given time and location. Spaceborne radars can do just this, but their error structure is complex. Therefore, evaluating space-borne radar precipitation delineation capabilities with methods like the Heidke Skill Score, which does not use bulk metrics, allows for a breakdown of skills at finer levels (at a particular rain rate and reflectivity).

By utilizing the HSS, it was shown that the precipitation delineation capabilities are more sensitive to changes in rain rate when the 2D-HSS profile is more vertically oriented, and more sensitive to changes in reflectivity when the orientation is more horizontal. In comparing each radar, both the TRMM-PR and GPM-DPR performed better than the GPM-KuPR across almost all reflectivity thresholds and rain rates, with an exception for the GPM-DPR at lesser reflectivity values, where the two radars were much closer in capabilities. The GPM-DPR performed slightly better than the TRMM-PR at high reflectivity across almost all rain rates, while the TRMM-PR performed better at lower reflectivity, most notably at lower reflectivity and low rain rates. The TRMM-PR reached the highest score overall, 0.7, followed by the GPM-DPR at 0.56, and the GPM-KuPR at 0.23, leading to the exploration of what variables could impact the overall performance of the radars.

Upon looking at different factors that could affect the skill, stratiform precipitation could have an impact on scores at higher rain rates and reflectivity values, while convective could have a slightly smaller impact on scores at low rain rates and reflectivity values. The region and zenith angle did not greatly affect the overall performances of the radars. The land surface type performed

the most similarly to the overall performance, while the ocean surface type could have a negative impact across all reflectivity values at low rain rates and across all rain rates at high reflectivity. The inland water surface provided a slightly positive impact on scores for the TRMM-PR across most rain rates and reflectivity values, while having a slightly negative impact on the GPM-DPR. The coast surface also decreased scores, but not significantly. Both the presence of the bright band and shallow rain could negatively impact the detection of precipitation. This impact is more significant with shallow rain. The bright band also had a negative impact on delineation skill at high reflectivity across almost all rain rates. Many of these factors, however, had a limited impact on the overall size due to a relatively small sample size.

This research shows that the GPM-DPR in particular struggles with the detection of precipitation, which could be impacted by a number of factors including the bright band and shallow rain. It also shows that some factors, such as region and zenith angle, do not have a significant impact, while other factors, such as the inland water surface type, had an opposite effect on the two radars. While the TRMM-PR does perform better than the GPM-DPR across most rain rates and reflectivity values, their overall scores both demonstrate good delineation capabilities.

References

Brier, G. W., and R. A. Allen, 1951: Verification of Weather Forecasts. *Compendium of Meteorology,* T. Malone, Ed., Amer. Meteor. Soc., 841-848

Chiu, J. C., and G. W. Petty, 2006: Bayesian Retrieval of Complete Posterior PDFs of Oceanic Rain Rate from Microwave Observations. *J. Appl. Meteor. Climatol.*, **45**, 1073-1095, https://doi.org/10.1175/JAM2392.1

Clark, M. P., and Coauthors, 2021: The Abuse of Popular Performance Metrics in Hydrologic Modeling. *Water Resour. Res.,* **57**, https://doi.org/10.1029/2020WR029001

Conner, M. D., and G. W. Petty, 1998: Validation and Intercomparison on SSM/I Rain-Rate Retrieval Methods over the Continental United States. *J. Appl. Meteor. Climatol.*, **37**, 679-700, https://doi.org/10.1175/1520-0450(1998)037<0679:VAIOSI>2.0.CO;2

Hou, A. Y., and Coauthors, 2014: The Global Precipitation Measurement Mission. *Bull. Amer. Meteor. Soc.*, **95**, 701-722, https://doi.org/10.1175/BAMS-D-13-00164.1

Iguchi, T., 2003: Spaceborne Precipitation Radars in TRMM and GPM. *Proc. 31st Conf. Radar Meteor.*, Seattle, WA, Amer. Meteor. Soc., 371-374, https://ams.confex.com/ams/pdfpapers/64544.pdf

Iguchi, T., and Coauthors, 2021: GPM/DPR Level-2 Algorithm Theoretical Basis Document. 238 pp, https://gpm.nasa.gov/sites/default/files/2022-06/ATBD_DPR_V07A.pdf

Iguchi, T., and R. Meneghini, 2017: GPM DPR Precipitation Profile L2A 1.5 Hours 13 km V05. Subset used: May 2014 – October 2016, Goddard Earth Sciences Data and Information Services Center (GES DISC), accessed 1 October 2020, http://dx.doi.org/10.5067/GPM/DPR/GPM/2A/05

Iguchi, T., T. Kozu, J. Kwiatkowski, R. Meneghini, J. Awaka, and K. Okamoto, 2009: Uncertainties in the Rain Profiling Algorithm for the TRMM Precipitation Radar. *J. Meteor. Soc. Japan,* **87A**, 1-30, https://doi.org/10.2151/jmsj.87A.1

Iguchi, T., T. Kozu, R. Meneghini, J. Awaka, and K. Okamoto, 2000: Rain-profiling Algorithm for the TRMM Precipitation Radar. *J. Appl. Meteor.*, **39**, 2038-2052, https://doi.org/10.1175/1520-0450(2001)040<2038:RPAFTT>2.0.CO;2

Kirstetter, P. -E., and Coauthors, 2012: Toward a Framework for Systematic Error Modeling of Spaceborne Precipitation Radar with NOAA/NSSL Ground Radar-Based National Mosaic QPE. *J. Hydrometeor.*, **13**, 1285-1300, https://doi.org/10.1175/JHM-D-11-0139.1

Kirstetter, P. -E., J. J. Gourley, Y. Hong, J. Zhang, S. Moazamigoodarzi, C. Langston, and A. Arthur, 2015b: Probabilistic Precipitation Rate Estimates with Ground-based Radar Networks. *Water Resour. Res.*, **51**, 1422-1442, https://doi.org/10.1002/2014WR015672

Kirstetter, P. -E., W. A. Petersen, C. D. Kummerow, and D. B. Wolff, 2020: Integrated Multi-satellite Evaluation for the Global Precipitation Measurement: Impact of Precipitation Types on Spaceborne Precipitation Estimation. *Satellite Precipitation Measurement,* V. Levizzani et al., Eds., Springer, 583-608, https://doi.org/10.1007/978-3-030-35798-6_7

Kirstetter, P. -E., Y. Hong, J. J. Gourley, M. Schwaller, W. Petersen, and Q. Cao, 2015a: Impact of Sub-pixel Rainfall Variability on Spaceborne Precipitation Estimation: Evaluating the TRMM 2A25 Product. *Quart. J. Roy. Meteor. Soc.*, **141**, 953-966, https://doi.org/10.1002/qj.2416

Kirstetter, P. -E., Y. Hong, J. J. Gourley, Q. Cao, M. Schwaller, and W. Petersen, 2014: Research Framework to Bridge from the Global Precipitation Measurement Mission Core Satellite to the Constellation Sensors Using Ground-Radar-Based National Mosaic QPE. *Remote Sensing of the Terrestrial Water Cycle, Geophys. Monogr.*, Vol. 206, Amer. Geophys. Union, 61-79, https://doi.org/10.1002/9781118872086.ch4

Kummerow, C., W. Barnes, T. Kozu, J. Shiue, and J. Simpson, 1998: The Tropical Rainfall Measuring Mission (TRMM) Sensor Package. *J. Atmos. Oceanic Technol.*, **15**, 809-817, https://doi.org/10.1175/1520-0426(1998)015<0809:TTRMMT>2.0.CO;2

Lakshmanan, V., T. Smith, G. J. Stumpf, and K. Hondl, 2007: The Warning Decision Support System-Integrated Information. *Wea. Forecasting*, **22**, 596-612, https://doi.org/10.1175/WAF1009.1

Lasser, M., S. O, and U. Foelsche, 2019: Evaluation of GPM-DPR Precipitation Estimates with WegenerNet Gauge Data. *Atmos. Meas. Tech.*, **12**, 5055-5070, https://doi.org/10.5194/amt-12-5055-2019

Liao, L., and R. Meneghini, 2022: GPM DPR Retrievals: Algorithm, Evaluation, and Validation. *Remote Sensing*, **14**, 843, https://doi.org/10.3390/rs14040843

Liu, Y., Y. Zheng, W. Li, and T. Zhou, 2022: Evaluating the Performance of Satellite-Based Precipitation Products Using Gauge Measurement of Hydrological Modeling: A Case Study in a Dry Basing of Northwest China. *J. Hydrometeor.*, **23**, 541-559, https://doi.org/10.1175/JHM-D-21-0152.1

NASA, 2020a: Precipitation Radar (PR) Accessed 20 May 2022, https://gpm.nasa.gov/missions/TRMM/satellite/PR

NASA, 2020b: Dual-frequency Precipitation Radar. Accessed 20 May 2022, https://gpm.nasa.gov/missions/GPM/DPR

NASA, 2021: GPM Science Objectives. Accessed 23 May 2022, https://www.nasa.gov/mission_pages/GPM/science/index.html

Porcacchia, L., P.-E. Kirstetter, V. Maggioni, and S. Tanelli, 2019: Investigating the GPM Dual-Frequency Precipitation Radar Signatures of Low-level Precipitation Enhancement. *Quart. J. Roy. Meteor. Soc.*, **145**, 3161-3174, https://doi.org/10.1002/qj.3611

Skofronick-Jackson, G., and Coauthors, 2017: The Global Precipitation Measurement (GPM) Mission for Science and Society. *Bull. Amer. Meteor. Soc.*, **98**, 1679-1695, https://doi.org/10.1175/BAMS-D-15-00306.1

Steiner, M., R.A. Houze, Jr., and S.E. Yuter, 1995: Climatological Characterization of Three-dimensional Storm Structure from Operational Radar and Rain Gauge Data, *J. Appl. Meteor.*, **34**, 1978-2007, https://doi.org/10.1175/1520-0450(1995)034<1978:CCOTDS>2.0.CO;2

Stephens, G. L., and Coauthors, 2002: The *CloudSat* Mission and the A-Train. *Bull. Amer. Meteor. Soc.*, **83**, 1771-1790, https://doi.org/10.1175/BAMS-83-12-1771

Tropical Rainfall Measuring Mission (TRMM), 2011: TRMM Precipitation Radar Rain Characteristics L2 1.5 hours V7, subset used: May 2011 – October 2011, Goddard Earth Sciences Data and Information Services Center (GES DISC), accessed 2 June 2022, https://disc.gsfc.nasa.gov/datacollection/TRMM_2A23_7.html

Valdivia, J. M., P. N. Gatlin, K. Shailendra, D. Scipión, Y. Silva, and W. A. Petersen, 2022: The GPM-DPR Blind Zone Effect on Satellite-Based Radar Estimation of Precipitation over the Andes from a Ground-Based Ka-band Profiler Perspective. *J. Appl. Meteor. Climatol.*, **61**, 441-456, https://doi.org/10.1175/JAMC-D-20-0211.1

Wolff, D. B., and B. L. Fisher, 2008: Comparisons of Instantaneous TRMM Ground Validation and Satellite Rain-Rate Estimates at Different Spatial Scales. *J. Appl. Meteor. Climatol.*, **47**, 2215-2237, https://doi.org/10.1175/2008JAMC1875.1

Yuter, S. E., and R. A. Houze, Jr., 1997: Measurements of Raindrop Size Distributions Over the Pacific Warm Pool and Implications for Z-R Relations, *J. Appl. Meteorol.*, **36**, 847-867, https://doi.org/10.1175/1520-0450(1997)036<0847:MORSDO>2.0.CO;2

Zhang, J. and Coauthors, 2016: Multi-Radar Multi-Senso (MRMS) Quantitative Precipitation Estimation: Initial Operating Capabilities. *Bull. Amer. Meteor. Soc.*, **97**, 621-638, https://doi.org/10.1175/BAMS-D-14-00174.1

Zhang, J., and Coauthors, 2011: National Mosaic and Multi-Sensor QPE (NMQ) System: Description, Results, and Future Plans. *Bull. Amer. Meteor. Soc.*, **92**, 1321-1338, https://doi.org/10.1175/2011BAMS-D-11-00047.1

Zhang, J., Y. Qi, C. Langston, and B. Kaney, 2012: Radar Quality Index (RQI) – A Combined Measure for Beam Blockage and VPR Effects in a National Network. *Weather Radar and Hydrology,* Moore R. J., S. J. Cole, and A. J. Illingworth, Eds., IAHS Publ. 351, 388-393.